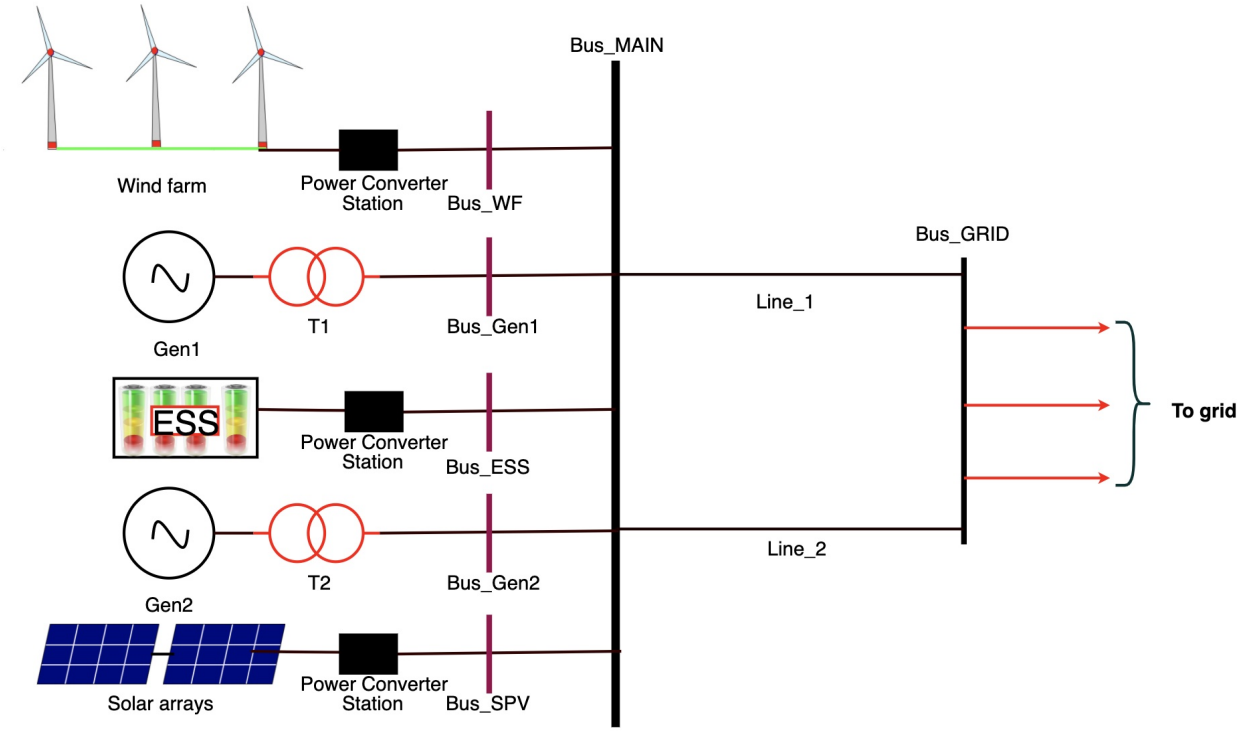

Frequency Control Support in Low Inertia Power Grid by Energy Storage Systems: A Techno-Economic Analysis

Master's thesis in Electric Power Engineering

Hafiz Zubyrul Kazme
Khwrwmdao Basumatary

DEPARTMENT OF ELECTRICAL ENGINEERING
Division of Electric Power Engineering
CHALMERS UNIVERSITY OF TECHNOLOGY
Gothenburg, Sweden 2021
www.chalmers.se

Master's thesis 2021

Frequency Control Support in Low Inertia Power Grid by Energy Storage Systems: A Techno-Economic Analysis

In the fulfilment of the Master of Science degree in Electric Power Engineering requirements, in the Department of Electrical Engineering.

Submitted by-

Hafiz Zubyrul Kazme
Khwrwmdao Basumatary

CHALMERS
UNIVERSITY OF TECHNOLOGY

Department of Electrical Engineering
Division of Electric Power Engineering
Chalmers University of Technology
Gothenburg, Sweden 2021

Frequency Control Support in Low Inertia Power Grid by Energy Storage Systems: A Techno-Economic Analysis

Hafiz Zubyrul Kazme
Khwrwmdao Basumatary

Examiner and Supervisor: **Associate Professor Anh Tuan Le**

Department of Electrical Engineering
Division of Electric Power Engineering
Chalmers University of Technology
SE-412 96 Gothenburg
Telephone +46 31 772 1000

Cover: Typical symbolic single line diagram of deploying energy storage system to a renewable dominated future electrical Grid.

Typeset in LaTeX
Printed by Chalmers Reproservice
Gothenburg, Sweden 2021

Abstract

Due to the intermittent nature of renewable energy sources like wind and solar power, curtailment of power from these generators is often required to keep the electrical grid stable. As more countries commit to decarbonization, however, the difficulty of integrating such intermittent sources into the grid becomes more important and complicated. Also, traditional power plants, such as thermal and nuclear, have large turbines that act as rotating mass, storing kinetic energy and acting as a safety net during disturbances in the grid. Hence, as we start to substitute such plants with power electronic converter dominated renewable power plants, which do not contribute any inertia and kinetic energy in the system, therefore, this loss in kinetic energy in the system makes the grid more unstable and vulnerable to disturbances.

The electrical grid contains various frequency containment reserves, predominantly from hydropower stations in the Nordic grid, designed to stabilize the grid whenever there is an imbalance between electrical energy generation and consumption. As renewable energy penetration increases, the reserves require more power to stabilize the grid. However, the cost for such an increase in power requirement increases exponentially. A solution to such a problem relies on utilizing Energy Storage Systems, which can provide the necessary power support very fast while keeping the cost lower than traditional systems when the power requirement is high. Such a solution addresses the imbalance of the grid and can provide proper support to reduce and/or eliminate the curtailment of renewable energy sources.

The Nordic-32 Test System was implemented in PSS®E for case studies where it was modified to capture the changes in renewable energy penetration in the future Nordic grid according to Nordic development plans. The results from the case studies have shown that: The performance of Energy Storage System for frequency regulation was better compared to hydro turbines as the conventional frequency support showing smaller initial frequency dip and flexible ramp up rates of power delivery from 17.2 MW/s to 25.9 MW/s when the renewable energy penetration in the system increased. Also, when the need for Frequency Containment Reserve-Disturbance (FCR-D) was higher than a certain level, 180 MW for this case study, a combined dispatch of power from traditional FCR-D sources and Lithium-ion battery based Energy Storage System achieved lower overall cost with predominantly higher percentage of power from the Energy Storage System, and when the requirement was higher than a certain level of 160MW in the case studies, the proportion of power from Vanadium Redox Flow Battery based Energy Storage System was higher than traditional FCR-D sources to achieve lower overall cost when a combined dispatch of them were taken into consideration. The overall cost of FCR-D can be reduced by at least 40% in cases with high FCR-D power requirement support.

Keywords: *renewable energy penetration, wind energy, solar energy, curtailment, decarbonization, kinetic energy, power imbalance, energy storage, ancillary service, FCR-D, performance, dispatch power combination, overall cost.*

Acknowledgements

We would like to express our utmost sincere gratitude to Associate Professor Anh Tuan Le for serving as our supervisor. We are grateful to have such a supportive mentor who encouraged us to pursue our ideas. Again, a big thank you to David Steen for sharing his knowledge of frequency control markets. We would also like to thank Professor Massimo Bongiorno for the consults and support during the thesis. We are indebted to Hannes Hagmar, because of him we have been able to complete our simulation studies; we are grateful to him for educating and guiding us throughout our simulation process in PSS®E.

I, Hafiz, would like to take this opportunity to first of all thank my father and my mother for their undying support throughout my academic career. A special thanks to my wife and our new born baby for giving me the mental strength and the emotional support I desperately needed throughout my journey of fulfilling my dream and achieving my masters degree. I am also grateful to Bangladesh Power Development Board (BPDB) for giving me the opportunity to make this possible.

I, Khwrwmdao, am very much thankful to my parents, who always encourage me to pursue higher studies abroad. Also, I am grateful to the Indian Embassy in Sweden for looking after me throughout my education, and especially to the Indian Government for providing me with the opportunity to pursue my higher education through a scholarship.

Special thanks to our friends, well wishers and family members who always motivate and inspire us when we need it the most.

Hafiz Zuburul Kazme
Khwrwmdao Basumatary

Gothenburg, September 2021

Contents

List of Figures

List of Tables

1
Introduction

1.1 Background

In the past, the world has experienced a sharp increase in carbon dioxide emissions, which has led to catastrophic environmental changes such as global warming, rise of sea level etc. For this reason, the modern world is intelligently evolving by turning away from fossil fuels and switching to renewable energy (RE) as the primary source of power production. The United Nations Sustainable Development Goals (UNSDGs) consist of various targets and goals to be achieved by 2030 and apply to all countries in the world. One of the goals, "Ensure Access to Affordable, Reliable, Sustainable and Modern Energy" [1], refers to significantly increasing the share of renewable energy in the global energy mix by 2030, thereby lowering the price of electricity and making it more affordable. However, integrating large amounts of renewable energy into the power grid is also a serious challenge.

The use of solar and wind energy has increased exponentially over the past decade, and this trend will continue if prices drop significantly [2],[3],[4]. The generation of electricity from solar and wind energy depends on solar irradiance and wind speed respectively. Since solar radiation and wind speed always fluctuate over time, the generation of electricity from such power plants also fluctuates. If solar and wind power are deployed on a large scale, such fluctuations would pose a serious threat to the stability and reliability of the power grid. The reduction of power generation from synchronous generators in combination with the intermittent behavior of power generation from the power electronic converter dominated solar and wind power plants reduces the inertia of the system causing the system frequency to deviate much higher or lower than the steady-state range. This, in turn, means the fluctuations between the generation and the demand of electrical energy in the grid, resulting in an increased occurrence of load shedding or blackouts.

The electrical grid uses various ancillary services to combat power fluctuations in total electrical power generation and consumption. Ancillary services refer to speciality services and functions that facilitate and support the continuous flow of electricity so that the demand for electrical energy in the system is met in real-time. Some examples of the ancillary services are Frequency Containment Reserve (FCR), Fast Frequency Response (FFR) and Frequency Restoration Reserve (FRR), which helps the grid to balance itself when there is an imbalance between generated and consumed power. FCR and FFR are the first responders when there is a change

in the system frequency and are enabled when the system frequency deviates from 50.0 Hz, and FRR is enabled after them. A premium must be paid for such services, which can cost much higher than the actual cost of power generation (average cost of household electricity is around 0.2417 €/KWh whereas the average cost of per unit FCR for disturbance service is about 11 €/MW [5]). With higher penetration of RE into the electrical grid, the frequency fluctuations become much higher and more frequent. The reliance and usage of FCR, FFR and FRR increase to mitigate such volatility, and since such services are quite costly, the overall power price may increase.

One solution to counter such frequency instability would be to extract the excess energy from solar and wind during peak generation periods and stored it in an Energy Storage System (ESS) to provide energy reserves for on-demand use during frequency fluctuations. In this report, a novel approach to find the dispatch composition for incurring lower overall cost for Frequency Containment Reserve for Disturbance (FCR-D) service is presented in which a combination of different ESSs in the form of fast acting Lithium-Ion Battery (LIB) and Vanadium Redox Flow Battery (VRFB) based ESS is used complimenting with the traditional FCR-D energy sources. In this way, the grid can become more reliable and also with the decrease in total cost of FCR-D service, the goal of affordable electricity can be achieved.

1.2 Aim

The objectives of this thesis are:

- To validate the increase in requirement of Frequency Containment Reserve for Disturbance (FCR-D) with increase in renewable energy penetration into the electrical grid.
- To evaluate the performance of an Energy Storage System (ESS) and compare its performance to that of a hydro turbine.
- To justify a suitable compliment for traditional sources of FCR-D support to gain economic advantages and attract future investors.

1.3 Tasks/Problems

- Conducting an in-depth literature review on the impact of high penetration of renewable energy sources into the electrical grid, and on the various ESS and Battery Management Systems (BMS) connected to the grid.
- Tune and validate models for ESS with power generation characteristics, according to Technical Requirement guidelines for FCR-D support, in the PSS®E simulation software.
- Developing scenarios in PSS®E software with penetration of renewable energy sources into the electric grid and perform dynamic simulation for Nordic-32 Test System to see the behavior and impact on frequency with N-1 contingency criteria disturbance.
- Test the Photo voltaic (PV) plant and wind turbine models as well as the ESS model on the Kundurs' test grid in the preliminary stage and later on

the Nordic-32 Test System with frequency regulation using hydro turbines and later with ESS.
- Develop a methodology to evaluate different dispatch combinations of traditional FCR-D source support with ESS as compliment to obtain lower overall cost of FCR-D support at different power requirement levels.

1.4 Scope and Organization of the thesis

This thesis looks into the behavior of a modified Nordic-32 test grid with varying renewable energy penetration levels during an N-1 contingency criteria disturbance where a generator is tripped and the resulting behavior on the system frequency is observed in the presence of primary frequency regulation. The modified grid consists of power plant units of solar and wind energy keeping the location of the plants according to scenarios specified by Nordic Development Plans. Numerical calculations would be performed to find the lower overall cost of FCR-D support using prices of traditional FCR-D service, obtained from historical data, and price of ESS with different energy sources obtained through Life Cycle Cost (LCC) calculations.

In this thesis, the following chapter provides the literature background towards Electrical Grid Frequency Stability, factors affecting it and the measures placed during disturbances. Later, **Chapter 3** discusses about Renewable Energy Penetration into the grid, its challenges and potential solutions for its drawbacks. **Chapter 4** discusses the methodology and working process of the thesis study and also testing and validating the models used for dynamic simulations in the Nordic-32 test system. **Chapter 5** would provide the case studies, scenarios and the observations from them with the following chapter providing the findings from the observations and results of different case studies and scenarios and also the calculations done during the process. Finally, **Chapter 7** would provde the conclusion and reflect on the overall results obtained from the studies and the objectives fulfilled while doing so.

2

Grid Frequency Stability

In this section, different terms related to frequency stability such as system inertia, kinetic energy, frequency dynamic swing equation, methods of frequency control, participation of TSOs in Nordic synchronous area and frequency regulation market have been briefly discussed.

2.1 Background on Frequency Stability

The electrical grid is a dynamic system which is always engaged in a tug of war between the amount of power generated by the generators and the amount of power consumed by the consumers. As the balance between them changes, so does various quantities associated with the electrical grid. The most noteworthy change due to the imbalance is observed in the system frequency. With higher imbalance, the system frequency deviates more from the normal or base value and if the frequency deviates more than a critical value, the electrical grid might fail to restore itself. Hence, frequency stability studies determines how much the grid is susceptible to changes and predicts its behavior to disturbances. To understand more on the dynamics of the frequency, we need to understand what are the contributing factors which lead to frequency imbalance. The following sections will provide in detail descriptions about the frequency dynamics of the electrical grid.

2.2 Frequency Dynamics

The grid frequency stability and its behavior can be mathematically expressed in various equations. The behavior of an electrical grid is fundamentally dependent on the Inertia and Kinetic Energy of the system which are used to express the Swing Equation of the system. The following sub-sections will describe these in detail.

2.2.1 Inertia and Kinetic Energy

This section discusses the basic terms and mathematical expressions related to inertia and kinetic energy, as well as how the behavior of power system frequency is influenced by them. According to European Network of Transmission System Operators for Electricity (ENTSO-E) [6], *"Inertia of a power system is defined as the ability of a system to oppose changes in frequency due to resistance provided by kinetic energy of rotating masses in individual turbine-generators"*, typically from hydropower plants [7]. Kinetic energy, on the other hand, is defined as the resistance to change in

motion of physical objects [12]. The term motion applies to the rotating machinery such as turbines, generators and induction generator and inertia corresponds to the change in speed of rotating masses [11], [12].

Frequency is affected by power fluctuations caused by a mismatch between power production and system demand. A slight change in power reflects in the form of frequency noise generated by rotating masses. However, when a sudden power deficit occurs due to tripping of a large generator, nominal frequency (50 Hz) start to change abruptly. The synchronously connected spinning masses strive to bridge the deficiency of power in order to maintain system in balance at all times. As a result, the kinetic energy stored in the rotating masses decreases, and the frequency decreases. However, for simplicity, in this study, it is assumed that the system's inertia is provided by kinetic energy stored in rotating masses of turbo-generator from a hydropower plant rather than the frequency dependent loads.

The inertia constant of a single synchronous machine in relation to the kinetic energy derived in [10], [13] as:

$$H = \frac{E_k}{S_r} \tag{2.1}$$

where S_r is the rated apparent power [VA], H is the inertia constant [s] and E_k is the kinetic energy stored in rotating mass of turbo-generator $[kg.m^2/s^2]$. Expanding eq. 2.1 as:

$$H = \frac{1}{2} \cdot \frac{J \cdot \Omega_{m,0}^2}{S_r} \tag{2.2}$$

where, J is the moment of inertia $[kg.m^2]$, $\Omega_{m,0}$ is the rated mechanical rotational speed $[rad/s]$.

In an interconnected power system containing of j^{th} generator units, the equivalent system inertia (H_{sys}) can be expressed as:

$$H_{sys} = \frac{\sum_{j=1}^{n} H_j \cdot S_j}{S_{sys}} \tag{2.3}$$

where, H_j and S_j are the inertia constant and apparent active power of j^{th} unit respectively and S_{sys} is the total generation capacity [11].

In other words, the summation of multiplication of inertia constant and apparent active power of j^{th} unit gives the kinetic energy. Hence, eq.(2.3) can be re-written as:

$$H_{sys} = \frac{\sum E_k}{S_{sys}} \quad [MWs/MVA] \tag{2.4}$$

Then eq.(2.3) or (2.4) can be simplified as:

$$E_{k,sys} = S_{sys} \cdot H_{sys} = \sum_{j=1}^{n} H_j \cdot S_j \quad [MWs] \tag{2.5}$$

where, $E_{k,sys}$ is the kinetic energy of the system.

Table 2.1 shows the Kinetic Energy capacity of the power system of Nordic countries in the Nordic Synchronous area with higher kinetic energy observed for Sweden.

Table 2.1: Kinetic energy capacity in each country's power system as per Nordic synchrnous area [14].

Country	Kinetic energy capacity in GWs
Eastern Denmark	30
Finland	90
Norway	100
Sweden	170
Synchronous system	**390**

2.2.2 Swing Equation

The frequency dynamic of a single generation unit subjected to power imbalance (Δp) can be described using the swing equation [15]. The majority of system inertia in power systems comes from turbo-generators of hydropower plants, thermal power plants and nuclear power plants which are synchronously connected to mechanical rotational speed (Ω_m) and directly connected to electrical angular frequency (Ω_e) [12]. Therefore, the motion of synchronously connected single generator unit defined in [10], [12] can be derived as:

$$J\frac{d\Omega_m}{dt} = T_m - T_e \tag{2.6}$$

where T_m and T_e represent mechanical and electrical torque in [N.m], respectively. J, on the other hand, defines the collective moment of inertia from turbine and generator in terms of electrical angular frequency, taking the number of pole pairs (p) into account [12]. With $\Omega_e = p \cdot \Omega_m$ and assuming p = 1, eq.(2.6) can be re-transform in terms of power instead of torque [13], [16] as:

$$\frac{d}{dt}\left(\frac{1}{2}J\Omega_m^2\right) = P_{gen} - P_{dem} \tag{2.7}$$

Likewise, as in the case of eq.(2.4) and (2.7), eq.(2.2) can be expanded to:

$$\Omega_m \cdot \frac{2H_{sys} \cdot S_{sys}}{\Omega_{m,0}^2} \cdot \frac{d\Omega_m}{dt} = P_{gen} - P_{dem} \tag{2.8}$$

Assuming, $\Omega_m = \Omega_{m,0}$ ($\Omega_{m,0}$ denotes the rated mechanical angular velocity in rad/s) for limited angular variation [16], eq.(2.8) can be re-derived as:

$$\frac{2H_{sys} \cdot S_{sys}}{\Omega_{m,0}} \cdot \frac{d\Omega_m}{dt} = P_{gen} - P_{dem} \tag{2.9}$$

Or,

$$\frac{2H_{sys}}{f_0} \cdot \frac{df}{dt} = \frac{P_{gen} - P_{dem}}{S_{sys}} = \frac{\Delta p}{S_{sys}} \tag{2.10}$$

Thus, simplifying eq.(2.9), we have-

$$\frac{df}{dt} = \frac{\Delta p \cdot f_0}{2E_{k,sys}} \tag{2.11}$$

where, f_0 is the nominal system frequency [Hz] and $\frac{df}{dt}$ is the rate of change of frequency (RoCoF) [13], [16]. The derived swing equation eq.(2.9) and (2.11) states the relationship between H_{sys} and RoCoF with nominal system frequency (f_0) during imbalanced caused by active power generation (P_{gen}) and power demand (P_{dem}) due to power deficit (Δp) [13], [16]. Δp represents the size of disturbance, which determines the initial RoCoF [17]. The correlation between the RoCoF and power deficit (Δp) or energy stored by the system in the form kinetic energy (E_k) is stated in the [17]. With larger power deficit or lower energy stored in the rotating mass, the higher will be the initial RoCoF. Thus, the derived relationship aids in understanding how the kinetic energy $E_{k,sys}$ counteracts the RoCoF when there is a power deficit (Δp) caused by an imbalance.

2.3 Methods of Frequency Control

The imbalance in the system power generation and consumption is a common phenomena which is needed to be kept in a strict margin and for this reason various methods are used to regulate the frequency of the grid. As an example, there is continuous change in the electrical energy consumption across each day where the consumption is maximum during the peak hours and minimum during the off peak hours and In anticipation of such events, the active power generation from the generators are increased or reduced automatically through governor control or manually through plant operation settings to keep the frequency in control. In addition, the electrical grid contains self-regulating loads, which have a frequency dependence factor, which means that the load changes when the system frequency changes, for example load increases when the frequency increases and decreases when the frequency decreases, thereby assisting in the frequency stability. Under Frequency Load Shedding (UFLS) can be enabled in the event of a severe frequency imbalance, in which the distribution side of the grid cuts off electrical supply to high-power consumers when the frequency falls below a predetermined reference point, in order to avoid a critical impact on the electrical grid.

However, the measures stated above are only activated during their respective scenarios whereas the grid system frequency changes continuously throughout the day. For this reason, various ancillary services are procured by the Transmission System Operator (TSO) to combat the deviations in the system frequency within a very short time frame. These are called frequency regulation reserves; these are of three types depending upon the range of frequency deviation at which they are activated and the time and sequence of their activation. They are:

- Primary Frequency Regulation.
- Secondary Frequency Regulation.

- Tertiary Frequency Regulation.

The objectives and the scope of this thesis are specific to primary frequency regulation and so detailed theoretical background would be provided on it and brief description with specifications would be provided for secondary and tertiary frequency regulation reserves.

2.3.1 Primary Frequency Regulation

Primary Frequency Regulation (PFR) reserves are the active power operating reserves with the purpose of balancing the system frequency in the event of sudden imbalances between generation and consumption. PFR is the first responder to changes in the system frequency and therefore is a fundamental element necessary to maintain the frequency in balance and increase stability. As stated in [18], PFR is procured in advance for every minute of the day, which activates automatically through a local signal control once the grid deviates from the base frequency of 50 Hz. The action time of PFR is from 10 to 30 seconds which occurs after the inertial response (5-10 seconds) [19], [20]. There are three types of PFR reserves which can be provided independently:

- Frequency Containment Reserve for Normal Operation (FCR-N), activated in the range between 49.90 Hz to 50.10 Hz.
- Frequency Containment Reserve for Disturbance (FCR-D) upwards, activated in the range between 49.90 Hz to 49.50 Hz.
- Frequency Containment Reserve for Disturbance (FCR-D) downwards, activated in the range between 50.10 Hz to 50.50 Hz.
- FFR, activated when the frequency dips lower than 49.7 or 49.6 or 49.5 Hz depending upon the activation strategy chosen by the provider.

Each product can be provided either as a linear function of frequency deviation or as an approximation of a linear function.

For FCR-N and FCR-D application, information required by TSO are: (*for Energy Storage based sources*)

- Rated apparent power [MVA].
- Rated energy capacity of the energy storage [MWh].
- Energy storage upper and lower limits [MWh].
- Technical description of the controller, including controller settings.
- Description of energy management, if applicable.

2.3.1.1 FCR-N

FCR-N is an automatic reserve that continuously responds to both positive and negative frequency deviations from 50 $\pm$ 0.1 Hz. The power generation from FCR-N has a linear power delivery trajectory boundary where the power delivery increases with increase in frequency deviation and is fully activated when the frequency is equal to or lower than 49.9 Hz. The FCR-N support shifts to consumption, increasing

the consumption linearly with change in frequency and fully activating when the frequency is equal to or higher than 50.1 Hz [22]. In the Nordic synchronous area, the usual activity volume reserve requirement of FCR-N for Sweden was 230MW in 2013 which increased to 240MW in 2021 [23], [24]. Table 2.2 shows the technical requirements for FCR-N as specified by Swedish TSO Svenska Kraftnät (SvK) [23].

Table 2.2: Technical requirement of Frequency Containment Reserve-Normal (FCR-N) stated by Swedish TSO [23].

• **Activation mode:**	• Automatically at frequencies within and above 50 ± 0.1 Hz.
• **Activation time:**	• 63 % of the steady state power response within 60 sec (Sweden). • 100 % should be activated within 180 sec.
• **Endurance:**	• minimum of 1 h (continuous activation).
• **Bid size:**	• Minimum of 0.1 MW.
• **Other:**	• Symmetrical product for Up and Down regulation.

2.3.1.2 FCR-D

FCR-D is another FCR product that is triggered automatically for larger frequency deviations. The FCR-D shall be activated between frequency 49.90 - 49.50 Hz and/or 50.10 - 50.50 Hz and shall continue to be kept active for at least 15 minutes or until its energy reserve is depleted completely [21]. According to Nordic System Operation Agreement (SOA), FCR-D should be capable enough to responding N-1 contingency criterion (i.e. level of security of the system which ensures that system can withstand during the largest generation trips) following trip of largest nuclear power plant Oskarshamn-3 of 1450 MW. In the Nordic synchronous area, the usual activity volume reserve requirement of FCR-D for Sweden was 411.8MW in 2013 which increased to 580MW in 2021 [23], [24]. Table 2.3 shows the technical requirements for FCR-D (up regulation) as specified by SvK [23].

Table 2.3: Technical requirement Frequency Containment Reserve-Disturbance (FCR-D) stated by Swedish TSO [23].

• **Activation mode:**	• Automatically at frequencies under 49.90 Hz.
• **Activation time:**	• 50 % should be activated within 5 sec. • 100 % should be activated within 30 sec.
• **Endurance:**	• minimum of 15 min.
• **Bid size:**	• minimum of 0.1 MW.
• **Other:**	• asymmetrical product for Up regulation.

- **FCR-D stationary performance requirements** –

The power delivery from the FCR-D upward and downward support should be according to the technical requirements mandated by Svenska Kraftnät [21]. Figure 2.1 shows the variation of power delivery of the FCR-D service provider as well as the acceptable boundaries of power delivery with change in system frequency.

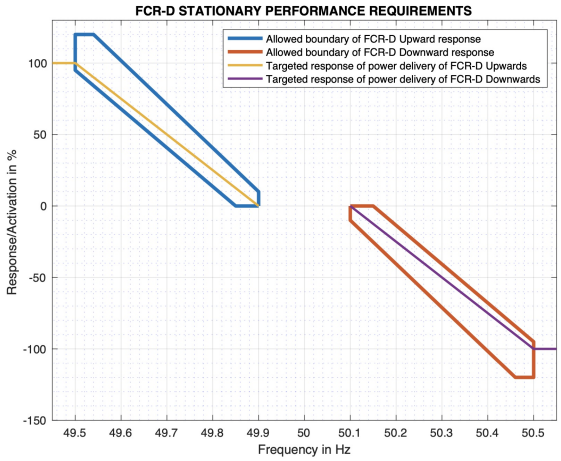

Figure 2.1: Activation of FCR-D (adapted from [21]). *In the figure, solid yellow and pink line (linear) indicates targeted response of power delivery of FCR-D Upwards and Downwards respectively; blue and orange line (piece-wise)indicates the allowed response of FCR-D Upwards and Downwards respectively.*

- **FCR-D dynamic performance requirement** –

The FCR-D dynamic performance requirement is based on the activated power and energy when the entity is subjected to a frequency input ramp from 49.90 Hz to 49.0 Hz, with a slope of -0.24 Hz/s for FCR-D upwards. For FCR-D downwards, the ramp is from 50.10 Hz to 51.0 Hz with a slope of 0.24 Hz/s. The requirements are:

1. $|\Delta P_{7.5s}| \geqslant 0.93 \cdot |\Delta P_{ss}|$
2. $|E_{7.5s}| \geqslant 3.7\text{s} \cdot |\Delta P_{ss}|$

where, $\Delta P_{7.5s}$ (MW) is the activated power at 7.5 seconds after applying the step signal, ΔP_{ss} (MW) is the steady state FCR-D activation power in case of frequency change from 49.90 Hz to 49.50 Hz (upwards) or from 50.10 Hz to 50.5 Hz (downwards) and $E_{7.5seconds}$ (MWs) is the activated energy provided starting from the ramp signal to 7.5 seconds after the start of the ramp. The energy can be calculated as:

$$E_{7.5seconds} = \int_{t}^{t+7.5seconds} \Delta P(t)dt \tag{2.12}$$

If the FCR provider fulfils the performance requirement, capacity is based on steady-state power. If the FCR providing entity does not satisfy the performance requirement, it can still be pre-qualified for the part of the capacity that meets the above-stated conditions. Then the FCR-D capacity, C_{FCR-D}, is calculated as the minimum of the three requirements for power activation performance, stationary performance and energy activation performance:

$$C_{FCR-D} = \mathbf{min}\left(\left|\frac{\Delta P_{7.5s}}{9.3}\right|, |\Delta P_{ss}|, \left|\frac{\Delta E_{7.5s}}{3.7s}\right|\right) \tag{2.13}$$

- **FCR-D deactivation performance** –

Deactivation is defined as the decrease in the FCR-D response when the frequency deviation decreases. FCR-D providing entities shall fulfil the exact requirements for deactivation requirements as stated previously in the conditions for dynamic performance requirements.

2.3.1.3 Fast Frequency Reserve

According to ENTSO-E [6], "*Fast-Frequency Reserve is a system service that delivers a fast power change to mitigate the effect of reduced inertial response, so that frequency stability can be maintained*". SvK launched this service back in 2020 [25]. ENTSO-E defined in [26] that FFR should only be for under frequency situations since it is more critical than over-frequency situations. The FFR is designed to compliment the FCR-D upwards when the kinetic energy in the system is low. When the kinetic energy in the power system is lower than the performance design limit for the FCR-D upwards, FFR is then needed to be procured to secure transient frequency stability. The example of new technology which is providing FFR includes converter-based technologies such as wind, solar photo-voltaic (PV), Battery Energy Storage System (BESS), HVDC connections and demand-side resources such as Battery Electric Vehicles [7], [11], [27]. Table 2.4 below shows a summary of the technical requirements of FFR support.

Table 2.4: Technical requirement of Fast Frequency Response (FFR) stated by Swedish TSO [23], [25].

• **Activation mode:**	• Activate automatically upon frequency deviation when kinetic energy of the system is low.
• **Activation time:**	To achieve 100 % activation, one of the following options must be selected: • Activation signal at 49.50 Hz with full activation within 0.7 sec. • Activation signal at 49.60 Hz with full activation within 1.0 sec. • Activation signal at 49.70 Hz with full activation within 1.3 sec.
• **Support duration:**	One of the following options must be selected: • Short term support of 5 sec. after full activation • Long term support of 30 sec. after full activation
• **Bid size:**	• Minimum of 0.1 MW.
• **Repeatability:**	• Ready for re-activation within 15 min.

2.3.2 Secondary and Tertiary Frequency Reserve

The Secondary and Tertiary Frequency Reserves behave similarly to Primary in terms of functionality, however, these are activated after it in sequence as shown in Figure 2.3. As stated previously, the PFR is the first responder during any changes in the system frequency and their main target is to minimize the deviation of frequency from its base value. So when the PFR is able to slow down the rate of frequency change into a steady value of system frequency, the Secondary Frequency Reserve (SFR) takes on the primary role of bringing the frequency back to a value close to the reference frequency and later shifts the role to Tertiary Frequency Reserve (TFR) which brings the frequency back to 50.0 Hz. In the complete sequence, there are overlaps between the different frequency reserves.

The SFR and TFR uses the service known as Frequency Restoration Reserve (FRR) where SFR uses Automatic Frequency Restoration Reserve (aFRR) while TFR uses Manual Frequency Restoration Reserve (mFRR). The action time for aFRR is from 30 seconds to 15 minutes and has a faster response than mFRR because it is founded on merit order and takes congestion into account in the Nordic synchronous grid and it is expected to be more prominent reserve in future while integrating intermittent and stochastic energy sources [7], [28]. In context to Sweden, the aFRR requirement in 2021 is 140 MW [23]. Table 2.5 shows the Technical requirements of aFRR stated

by Swedish TSO SvK.

Table 2.5: Technical requirement Frequency Restoration Reserve-automatic (aFRR) stated by Swedish TSO [23].

• **Activation mode:**	• Activates automatically centrally when the frequency drops from 50 Hz (when aFRR is procured)
• **Activation time:**	• 100 % should be activated within 120 sec.
• **Endurance:**	• Minimum of 1 h
• **Bid size:**	• Minimum of 5 MW.

The mFRR, on the other hand, relieves aFRR from its role after a prolonged disturbance and is activated manually at SvK's request when the frequency falls below the nominal frequency of 50 Hz, due to forecasted imbalances [7], [18], [24]. The mFRR is used to replenish the active power of spinning and other energy storage reserves that were depleted during PFR and SFR and to ensure that these reserves are distributed optimally [19]. The main balancing resource, the mFRR, activates in 15 minutes and lasts for 60 minutes [19], and is used for power balancing and congestion management in both normal and disturbance conditions, replacing the FCR and aFRR reserves and restoring frequency to the target level. According to [28], when pro-active activations occur, the mFRR can activate in the opposite direction of FCR and aFRR. Despite the fact that aFRR has a faster response time than mFRR, the Nordic synchrnous area tends to rely on mFRR as the primary balancing resource in the system due to small aFRR volumes and numerous grid congestions. Table 2.6 shows the Technical requirements of mFRR stated by SvK.

Table 2.6: Technical requirements for Frequency Restoration Reserve-manual (mFRR) stated by Swedish TSO [23].

• **Activation mode:**	• At the request of Svenska Kraftnät, manually.
• **Activation time:**	• activated within 15 min.
• **Endurance:**	• Minimum of 1 h.
• **Bid size:**	• Minimum of 10 MW.

2.4 Transmission System Operators (TSOs)

The Nordic grid electric power supply has been gradually expanding from late 19th century to the beginning of the 20th century where, small local electrical companies started to merge together to become larger regional units and eventually, the Nordic grid developed to such a position in which the electrical power grids of individual countries linked together via high voltage interconnections to share their power with each other.

The Nordic countries have different production system when it comes to electricity generation. The country of Denmark has majority of production from thermal and wind power, whereas Sweden and Finland have a mixture of nuclear and hydropower and Norway has a large amount of hydropower only. The system connecting Finland, Norway, Sweden, and Denmark constitutes a single area with a common frequency. This synchronous interconnection is called 'Synchronized system'. Another portion of Western Denmark is connected to Norway and Sweden via HVDC links. Together, these two systems comprise what is known as the Nordic Electric Power System. Through collaboration, the Nordic electric power system provides better security and lower costs, reduces the need for reserves and improves the potential for obtaining support during severe disturbances caused by natural calamity or through shortage of fuel [30].

The Nordic Electric Power System consists of four Transmission System Operators (TSOs) which govern their individual country's as well as the interconnected electrical system.

- **Energinet** – An independent public enterprise owned by the Danish Ministry of Climate, Energy and Utilities. They regulate the electrical power grid of Denmark.
- **Fingrid** - Finnish state and Finnish pension insurance companies owned transmission system operator. They regulate the electrical power grid of Finland.
- **Statnett** - Statnett is the system operator in the Norwegian energy system. it is a state enterprise owned by the Norwegian state through the Ministry of Petroleum and Energy. They regulate the electrical power grid of Norway.
- **Svenska Kraftnät** – It is an authority that is operated in the form of a state-owned enterprise. The operations are mainly funded by the revenue that they receive for their services. They regulate the electrical power grid of Sweden.

The table below summarizes some of the parameters of individual TSOs in Nordic synchronous area.

Table 2.7: Data corresponding to the individual TSOs [31].

TSO	Controlled Country	Approx. Circuit length, Km	Power Prod. Sources	Voltage level (400-380) kV	Voltage level (220-150) kV	Voltage level (132-50) kV
Energinet	Denmark	6,800	Wind, Thermal	28 (%)	48 (%)	24 (%)
Fingrid	Finland	14,000	Hydro, Thermal	31 (%)	17 (%)	52 (%)
Statnett	Norway	11,000	Hydro	73 (%)	0 (%)	27 (%)
Svenska Kraftnät	Sweden	17,000	Hydro, Thermal	69 (%)	26 (%)	5 (%)

2.4.1 Frequency Regulation in the Nordic Grid

According to IEEE/CIGRE tasks force, frequency stability can be defined as "*The ability of a power system to maintain steady frequency following a severe system upset resulting in a significant imbalance between generation and load*" [32]. The largest reference incident in the Nordic power system is tripping of the nuclear power plant Oskarshamn 3 of 1450 MW. To ensure the operational security and reliable system, the system frequency in Sweden as a part of Nordic power system allows to vary within band of 50 ± 0.1 Hz [11], [20]. The frequency stability is mainly dependent on three factors namely kinetic energy of the system, available reserves and size of the dimensioning incident.

- **Nordic power grid frequency control processes -**

There are several stages of frequency response reserve deployment in Sweden who is a part of ENTSO-E. The mismatch in generation to consumption of power gives rise to disturbance which can be categorized based on magnitude, endurance and speed [28], [33]. Figure 2.2 shows the illustration of various stages of frequency response defined by ENTSO-E and SvK.

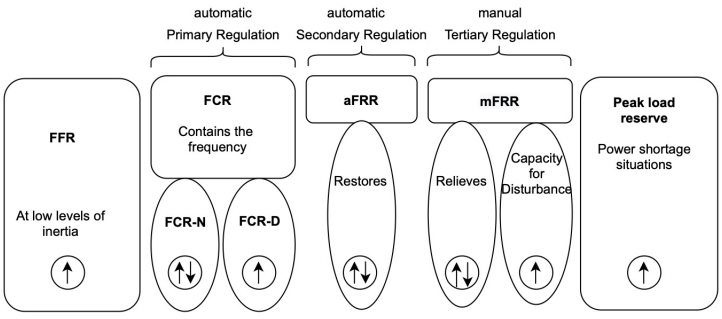

Figure 2.2: Class of frequency regulation market defined by ENTSO-E and Svenska Kraftnät (adapted from [23]).

The first stage is the inertial response from the system. When a power imbalance occurs due to dimensioning incidence (DI) at t=0 sec, the synchronous machines can detect the power deficit and attempt to change the rotational speed naturally to restore generation and demand by releasing the kinetic energy (E_k) stored in the rotating masses of turbines of synchronous machines for 5–10 seconds [20]. As a result, machine starts slowing down for which the frequency drops. The minimum frequency deviation termed as frequency nadir point is defined by the inertial response [15]. Following the inertial response, the PFR takes over, arresting the minimum frequency deviation and stabilizing it to a steady state frequency lower than the nominal system frequency. The magnitude and timing of PFR deployment have an impact on the frequency nadir in the grid to avoid load shedding and concurrent power blackouts [13]. After PFR, SFR takes over, typically recovering the PFR and bringing frequency back to a normal range within 49.90 Hz. Finally, TFR aids in the complete restoration to the nominal frequency value of 50 Hz and prepares for the next disturbance. Figure 2.3 illustrates this complete process.

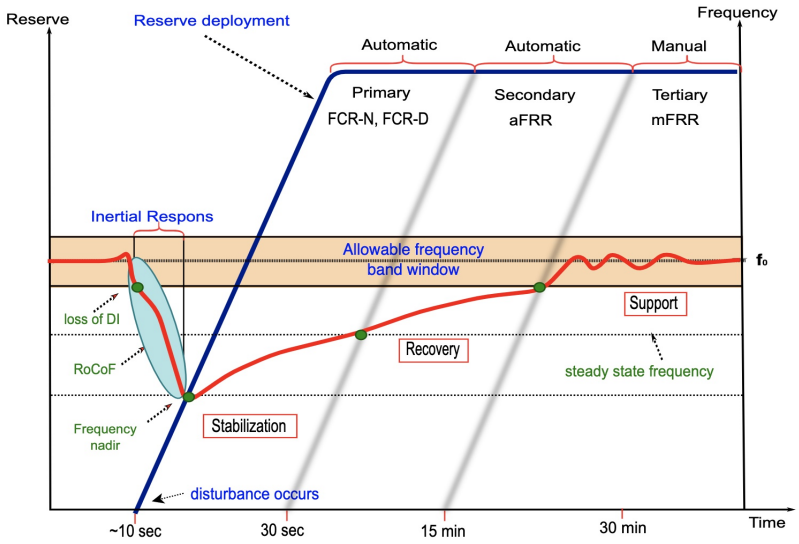

Figure 2.3: Frequency Response stages defined by ENTSO-E. (adapted from [13]).

2.4.2 Nordic electricity market

The Nordic electricity market consists of several markets for trading electricity, including the day-ahead market (Elspot), intra-day market (Elbas), and balancing market.

Day-Ahead-Market (Elspot) also known as the spot market, is where majority of the electricity is traded in order to match the everyday supply and demand. On the basis of hourly blocks of the day, customer or energy trader offer bids for buying or selling for the next 24 hours. The spot price (system price) and volume of energy are negotiated as per the point where both supply and demand cumulative curve intersects each other as illustrated in Figure 2.4 which gives an idea of the spot market. The system price is the common price for Nordic synchronous area for all hours of the next following 24 hours periods [35].

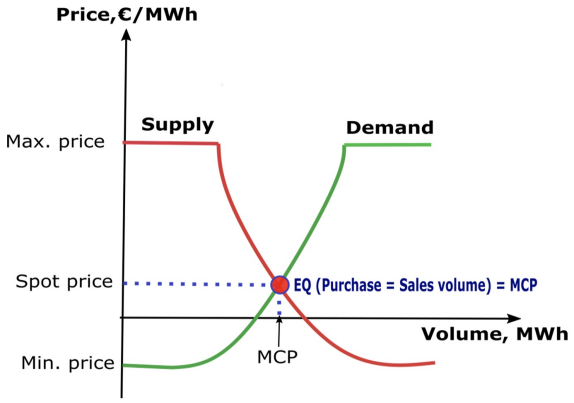

Figure 2.4: Day-ahead spot market calculation. Equilibrium (EQ) is the point of intersection between supply and demand that represents the best trade for the market clearing price (MCP) (adapted from [34]).

Intra-Day-Market (Elbas) : Trades during the Day-Ahead-Market depends on the forecast of energy supply and demand, which could often vary due to weather conditions (i.e plant outages or change in wind power generation, etc.). Hence, Intra-Day-Market is a large platform for Balance Responsibility Party (BRPs) for compensating the inadequacy of power supply and demand volume that are dealt during the Day-Ahead-Market. This market ensures continuous trading to balance the day-ahead market's inadequacy. Nord Pool spot market is responsible for **Elspot** and **Elbas** market within Nordic synchronous area.

Balancing market: Nordic TSOs are responsible for trading and sharing the reserves within Nordic synchrnous area. In this market ancillary service such as automatic reserve (FCR-N, FCR-D and aFRR) and manual reserve (mFRR) used by Nordic TSOs are traded in order to balance the power system operation. The guidelines governing with Nordic balancing philosophy are stated in [28]. Nordic TSOs (Svenska Kraftnät, Fingrid, Energinet and Statnett) are responsible for balancing market. The details of Nordic balancing market is discussed in [29].

3

Renewable Energy Integration: Statistics, Challenges and Solutions by Energy Storage Systems

3.1 Background on Renewable Energy and its Sou− rces

Throughout the decade, solar and wind energy's global installed power capacity has grown exponentially [2] and this trend is expected to continue as the cost of solar PV modules and wind turbines fall [36], [37], [38]. According to Vattenfall, wind and solar generation are the least expensive of all renewable energy sources [39]. Wind turbines capture energy from the wind that flows through their blades and converts it into mechanical energy, which is then converted into electrical power by the generator. On the other hand, solar PV cells capture solar irradiation and convert it into voltage and current, which are then converted into usable electricity when fed into an inverter. Because wind speed and solar irradiation vary depending on the weather, the electricity generated from these sources fluctuate annually over time [40], making the grid more unstable as more of these sources are integrated into it. Also even though the recent trend of consumers are moving into all electric systems for economic reasons, but on the other hand, such change causes an increase in electricity demand to the point where transmission lines, which are already operating at near maximum capacity and voltage stability limits, has an increased possibility of voltage collapse [41], [42].

3.2 Statistics and Historical Data

According to IEA, the installed power generation capacity of solar PVs would increase from 1.0 GW from 2000 to 3142 GW worldwide and for wind power, the figure would increase from 17.0 GW to 1856 GW [2], The report from IEA shows how the modern world is intelligently evolving by turning away from fossil fuels and switching towards RE as the primary source of energy by 2040. Literature [2],[3],[4] pointed out that the use of solar and wind energy has increased exponentially over the past decade and this trend will continue with fall in the price significantly.

3.3 Future Direction of Development

The amount of solar and wind power capacity fed into the global electrical grid is rapidly increasing, and it is expected that by 2050, wind and solar energy combined will account for 50% of total energy production. According to World Economic Forum [43], Sweden has set an ambitious goal of achieving 50% efficient energy use by 2030, 100% renewable power production capacity by 2040, and net zero greenhouse gas emissions by 2045. According to the IVA Electricity Crossroads Project Report [44], the amount of wind power would increase from 15 TWh (2014) to 55 TWh (2030-2050) and the amount of solar power would increase from approximately 0 TWh (2014) to 15 TWh (2030-2050). In the System Development Plan 2018-2040 [7], SvK measures the power system scenario in 2040, which shows that the decommissioning of nuclear power plants and other thermal power plants reduces system inertia, causing frequency changes and system instability in the Nordic power system [7]. The increasing generation capacity from intermittent energy sources necessitates greater flexibility in the power system. In contrast, the system's inertia support will decrease by 2040 compared to 2020, as wind and solar power generation contribute no system inertia [7]. According to SvK, the gradual decommissioning of nuclear plants by 2040 will reduce mean annual kinetic energy to 159 GWs by 2040, down from 202 GWs in 2020 [7]. In the event of excess power generation, power will be reduced from hydropower plants due to the zero marginal or subsidy generation cost available to wind and solar power.

As per SvK's scenario, by 2040, the southern part of Sweden will be vulnerable to a significant number of power shortages (around 2600 MW), or nearly 400 hours per year [7]. To ensure the safe operation of the future power system while unlocking intermittent electricity generation, flexibility in both electricity generation and consumption is required. However, it is unspecified how much flexibility will be required to adjust a large amount of power adequacy, as stated in [7]. The increased share of solar and wind power in future total power statistics indicates that the Nordic electrical grid will experience severe frequency and voltage instability, and the FCR will play a critical role in keeping the electrical grid stable and operational. It is also unclear whether the amount of FCR that the country currently has in place will be sufficient to stabilize the electrical grid with such large amounts of solar and wind power integrated.

The question now arises whether the price of electricity would be low enough to satisfy the UNSDGs of affordable and reliable energy even though the usage of FCR (and so the amount spent on FCR) increases? Also, is there any way of ensuring the proper utilization and low curtailment of solar and wind power even with their intermittent generation nature?

3.4 Challenges of Renewable Energy Penetration into Electrical Grid

3.4.1 Power system instability

From previous chapters, it was understood that the electrical grid depends on the methods of frequency control, most notably on FCR support. In terms of stability analysis of the grid, the FCR is deemed as the regulating strength of the grid. The regulating strength is also equivalent to frequency bias factor (FBF) which is the activated steady-state power changed divided by the frequency change. So, in terms of frequency stability, an increased regulating strength reduces the frequency deviation in the first frequency swing and also decreases the steady-state frequency deviation. However, looking through a subject of closed-loop stability, too high regulating strength may result in decrease in stability margin making the system potentially more unstable.

The regulating strength denoted by (λ), which determines the steady-state frequency error defined in [13] as:

$$\lambda_{FCR} = \frac{\Delta p}{\Delta f_{ss}} \quad [MW/Hz] \tag{3.1}$$

where, steady-state frequency (Δf_{ss}) is the absolute value of frequency deviation following the occurrence of an imbalance of power (Δp), after the system frequency has been stabilized. Assuming that frequency deviation (Δf) corresponds to Δf_{ss} difference from nominal frequency (f_0) the equation (3.1) can be expressed as-

$$\lambda_{FCR} = \frac{\Delta p}{\Delta f} \tag{3.2}$$

The primary driving force towards the instability of the grid can be due to unwanted dynamics which is present in the response of the primary reserves. These dynamics cause a phase shift in the total transfer function which is seen as a delay between the input and the output signal and when combined with high amplification of the signal, the result can cause the response of the reserves to be ineffective and also aiding the system towards instability.

The system inertia resists frequency change, but in turn causes a phase shift; meaning, it takes some time before a frequency deviation is seen by the controller of the primary regulation. The deviation has to be large enough for the controller to identify the frequency change and adjust its control signal. With an ideal proportional primary frequency control, the controller can react without any delay and in proportion to the frequency deviation which would not cause any closed-loop instability with increased regulating strength. However, if the controller is affected by dynamics, high regulating strength will cause the controller to respond too much and with the delay in the response due to dynamics, can make the controller react such that it amplifies the output leading to frequency oscillations with growing amplitude and inevitably to an unstable condition. By looking at stability as a linear closed

loop, a Nyquist diagram can be used to explain the reasons behind the impact from increased regulating strength and conclude that the maximum regulating strength is a function of the kinetic energy in the system.

The loop gain derived from the Nyquist plot in [6] is given by-

$$G_o(j\omega) = F(j\omega)G(j\omega) = \lambda_{FCR}F(j\omega)G(j\omega) = \lambda_{FCR}F_o(j\omega)\frac{\frac{f_0}{S_r}}{2H_{sys}j\omega + kf_n} \quad (3.3)$$

where,
$F_o(j\omega)$ = Transfer function of the FCR-D with gain one at steady-state.
H_{sys} = Total inertia of the system.
$j\omega$ = Complex angular frequency.
f_0 = Nominal frequency.
λ_{FCR} = Continuously-controlled regulating strength.

With reduced inertia in the system, the regulating strength has to be adjusted accordingly to keep a certain stability margin. Thus if the system inertia goes down below a certain minimum, the regulating strength has to be reduced as well. In the project Revision of the Frequency Containment Process (FCP), a stability margin is introduced for a minimum kinetic energy of 120 GWs in the system. In the Nordic synchronous area, the current volume requirement for FCR-N is at least 600 MW at a frequency deviation of 0.1 Hz, and the volume requirement for FCR-D is 1450 MW at an additional frequency deviation of 0.4 Hz [6].

The regulating strength requirement for the frequency deviation or rise within 50 ± 0.50 Hz is-

$$\lambda_{FCR-D} = \frac{1450\ MW}{0.4\ Hz} = 3625 \quad [MW/Hz] \quad (3.4)$$

Also, the regulating strength requirement for the frequency deviation or rise within 50 ± 0.10 Hz is-

$$\lambda_{FCR-N} = \frac{600\ MW}{0.1\ Hz} = 6000 \quad [MW/Hz] \quad (3.5)$$

- **Reduced regulating strength for kinetic energy below 120 GWs :**

For robust stability, the ratio between λ and H has to stay the same or below the original value. For instance, if the inertia is reduced to 90% from the minimum system value, a reduction of regulating strength to 90% guarantees robust stability. It should be noted that, after the dimensioning incident, the loss of kinetic energy in the system due to the disconnections has to be subtracted from the total kinetic energy before the incident. If the kinetic energy is reduced from 120 GWs to a value of X, the regulating strength has to be reduced accordingly to maintain the stability margin:

$$\lambda_{FCR-D_{(reduced)}} = 1 - \frac{120\ GWs - X}{120\ GWs} \cdot \lambda_{FCR-D} \quad (3.6)$$

3.5 ESS : Solution to Higher Renewable Energy Penetration

As we have already seen from the previous chapters that with higher renewable energy penetration, the electrical grid becomes more unstable due to loss in kinetic energy reserve in the network. Hence, it is of utmost importance to bring back reserve energy into the network and keep the system as stable as possible. The solution is to implement a source of energy which would activate when there is an imbalance between the total electrical energy generation and the total electrical energy consumption. The source could either fill in the lack of electrical energy in the grid or consume and store the excess electrical energy from the grid to be activated in later disturbances. The energy source is cascaded with a converter and a controller, the whole scheme is known as an Energy Storage System (ESS). The converter and the controller can be of many types depending on the type of energy source to be used inside the ESS, however, the basic functionality and working principle remains similar.

3.5.1 Benefits of ESS

The ESS can be designed and scaled according to the application and needs for the electrical grid. There are many possibilities and benefits of using ESS and are described in brief below:

(a) The ESS can be used not only for frequency regulation but for voltage regulation as well. The amount of active and reactive power required to keep the voltage within a stable window can be extracted from the energy source of the ESS and the converter and controller will determine how much power is required and how much voltage is needed to be increased during voltage dips or interruptions.

(b) The ESS can also be used as a peaking power plant which can provide electrical power during peak times, also known as peak shaving, to keep the balance between generation and consumption. As such systems store their energy from the grid during off-peak times, they can deliver electrical power during peak times, profiting during the process. However, the active time of the system can be low or high according to the scale of the ESS.

(c) The ESS is very versatile since it can be scaled according to the requirement of the application. Since it is only composed of three main components (energy source, converter, and controller), the option to expand and increase its capacity is, in theory, quite straight forward.

(d) The ESS can also be implemented using a mixture of energy sources to satisfy different requirements of applications such as fast response time, high capacity within a budget, high power rating and so on.

3.5.2 Components of ESS

An Energy Storage System (ESS) can consist of many different energy sources, however, the components required to allow the energy source to provide power to the grid is relatively similar. The architecture and design of an ESS can be different depending upon its application but the major components which are essential in an ESS are listed below:

- Energy Source (typically Battery)
- Grid-connected inverter or Power
- Conversion System (PCS)
- Isolation transformer
- Protection devices
- Cooling system
- Control system
- Battery Management System (BMS)

The energy source can be of many different types which will be discussed later in the chapter. However, in brief, the energy source could contain either mechanical energy, chemical energy, electrochemical energy or thermal energy. The source is the most expensive part of the ESS and needs to be sufficient enough to satisfy the application as well as all other specifications of the ESS that are dependent upon the energy source.

The Grid-connected inverters or Power Conversion System (PCS) are of different topologies which can be broadly divided into Voltage Source (buck) type, Current Source (boost) type or Z-source (buck-boost) type. The inverters can also have other characteristics such as hard-switched or soft-switched, two-level or multilevel and interleaved or un-interleaved inverter. The current source inverters and soft switched type inverters are seldom used in grid scale application. The most common type of PCS are the hard-switched voltage source inverters, and they are popular because of its simplicity and high reliability. The B6 type inverter is the simplest and requires only six switches to operate, however, they suffer from high switching losses, high di/dt and harmonics. The drawbacks of the B6 type inverters can be overcome with multi-level inverters which reduces the voltage across each individual switches, increasing the overall voltage level of the inverter and so with high switching frequency the harmonic distortions can be drastically reduced. The drawback is however the complexity of modulation and control techniques which can also be eliminated through high performance computing which is easily available in today's market. The schematic of the above-mentioned topologies are briefly described in [45].

The Isolation Transformer is a device connecting the entire energy storage system to the grid. The transformer is rated according to the power rating of the ESS and the voltage rating of the point of common coupling (PCC) to the grid. The transformer can also have various vector groups or connection types depending upon the application and usage.

The Protection devices are required to keep the ESS unharmed and ride-through any disturbances that occur in the electrical grid. It mainly consists a combination of relays, isolators and circuit breakers which can act quickly and reliably to avoid malfunction and possible damage to the ESS.

The cooling system is an integral part of the ESS since it helps the complete system to be stable and operating in the best possible conditions. Since large amount of power and energy is being drawn from the system, heat energy is produced in large quantity which would increase the temperature of the system and the risk of hazards such as melting of devices or fire. To avoid such scenarios, the cooling system is designed such that it should be sufficient to extract the heat from the system evenly and efficiently. The cooling system should also be able to maintain a steady operating temperature of the system for it to work at its optimum level of performance and reduce the chances of failures of electronics.

The control system and the Battery Management System (BMS) work hand in hand in the operation of the ESS. The control system is the one which maintains the authority of power delivery of the ESS into the grid. Different algorithms and loop controls are placed in such a way that it obeys all the provisions required for its delivery as well as keeping the system intact and healthy. The control system has to exchange information with the BMS to understand the state of energy storage and plan ahead over the output of the ESS. The BMS can provide various data to the control system as well as operate its own process to keep the system healthy [46].

The BMS can:

- Minimizing temperature gradients across the system
- Protect the cells from internal degradation and capacity fade
- Provides optimal charging patterns
- Balancing cells throughout the stack.

3.5.3 Types of Energy Sources used in ESS

The types of energy storage technologies can be broadly classified into four categories: Mechanical Energy Storage Systems (MES), Electrochemical Energy Storage Systems (ECES), Chemical Energy Storage (CES) and Thermal Energy Storage Systems (TES). However, the systems described in the following sections have electrical energy as its input and output. For this reason, the systems in focus is ECES.

The ECES systems utilize electrochemical energy in systems such as batteries which store energy as chemical energy and converts it to electrical energy to transfer energy and power when required. Some examples of ECES are Lithium-ion Batteries (LiB), Lead-Acid Batteries (PbA), Nickel-Cadmium Batteries (Ni-Cd), Vanadium Redox Flow Batteries (VRFB), Sodium Sulfur Batteries (NaS) and Super-capacitors. For this thesis study we would use only two types of ECES namely: Lithium-ion batteries (LIB) and Vanadium Redox Flow Batteries (VRFB) due to their advanced development, scalability for large grid-scale applications and also for their reasonable

price point.

3.5.3.1 Lithium-ion (Li-ion) Battery

Lithium-ion battery is the most used energy source for a grid connected Battery Energy Storage System (BESS) because of its high energy density, stability, and high-power capacity. It also has high efficiency and cycle life compared to other traditional batteries such as Lead-Acid or Nickel-Cadmium batteries.

The Lithium-ion battery is made up of a Cathode, an Anode, a Separator, and an Electrolyte in which all the mentioned elements are submerged, and two current collectors connected to each of the electrodes. The cathode can be of different materials such as Lithium-Iron-Phosphate (LFP), Lithium-Manganese-oxide (LMO), Lithium-Cobalt-oxide (LCO), Lithium-Nickel-Manganese-Cobalt oxide (NMC) and Lithium-Nickel-Cobalt-Aluminum oxide (NCA) [47]. The anode commonly contains graphite due to its low cost and provides high potential difference for the battery. The separator is a semi-permeable membrane which is used to separate the cathode from the anode but allowing the flow of ions through it and the electrolyte is the medium through which the ions move from one side to the other.

- **Working principle of Lithium-Ion battery:**

When a lithium-ion battery is fully discharged, the lithium ions are intercalated into the cathode in a regular pattern. When the battery is being charged, the external voltage causes the lithium in the cathode to lose electron, deintercalated and move towards the anode where it intercalates by accepting an electron. This process continues until the cathode is no longer able to release any further lithium ion from it and keep a stable structure. During discharge of the battery, the process is reversed, the anode releases lithium ions to the cathode where it is intercalated, generating a flow of electrons from one side to the other [48]. The current goes through the device which is connected to the battery providing electrical energy to it.

The potential difference between the cathode and the anode of the lithium-ion battery causes the current flow and transfer of electrical power to or from the device. However, the potential difference between the cathode and the anode changes as more lithium ions are deintercalated from one electrode and intercalated into the other. As described previously that the intercalation process can only continue until the electrode structure is stable enough and so a margin of safety is considered. The voltage range of the battery as well as the capacity of the battery is defined by this margin. Lithium-ion battery with NMC as cathode and graphite as anode, the voltage of the battery increases as it is charged, and the charging continues until it has reached its voltage limit. This limit also signifies how much of charge has been stored in the battery which is called the State-of-Charge (SOC) of the battery.

- **Ageing of Lithium-ion battery:**

The lithium-ion batteries are also prone to degradation with changing operating conditions. During its lifetime, the battery would go through mainly two types of ageing: Calendar ageing and Cycling ageing.

Calendar ageing: Calendar ageing refers to the degradation of the battery when it is left unused for a period of time. The internal chemistry of the battery, when left unused, is at a steady state such that the forward and the reverse chemical reactions are equal which means the battery would degrade over time. The calendar ageing is influenced by some environmental factors as well with temperature being the most influential factor. The calendar ageing is accelerated at higher temperatures and vice versa. So, if left unused for a long period of time, storing in a cold place would improve the battery's lifetime substantially [49].

Cycling ageing: Cycling ageing refers to the degradation of the battery when it is in use. The batteries have a pre-defined number of life-cycles given by the manufacturer stating that the battery would lose significant percentage of its capacity after the defined cycles of use. The cycling ageing is also influenced by many factors and it depends upon the environment as well as the way the battery is being used [49].

Depth of Discharge (DOD) is one factor which influences the ageing process. DOD refers to the percentage of SOC the battery has been depleted to at each cycle. For instance, if the battery is cycled from 100% SOC to 10% SOC, that means the DOD is 0.9 and the maximum value of DOD can be 1.0 for full usage of the SOC window. If the usage DOD is high, the ageing process is much faster compared to lower usage DOD.

Charge/Discharge current is another factor which is a major influencer in the ageing process. The cycle current is denoted by C-rate. With 1C rate, the current is the amount which is specified by the manufacturer. 2C rate denotes twice the specified current and ½ C rate denotes half of the current specified. With fast charging and discharging, the cycle current is between 4C to around 10C which speeds up the ageing process substantially and with lower C rate, the ageing process can be slowed down.

Temperature also contributes to the cycling ageing of the battery. However, during cycling, lower temperature causes the internal resistance of the battery to increase which can cause higher ageing. On the other hand, higher temperature causes the internal resistance of the battery to decrease which can slow down the ageing process.

The main advantages and disadvantages Lithium-ion (Li-ion) are as follows:

Advantages	Disadvantages
• Commercialized technology.	• Cost is still high.
• Fast charging and extended cell life.	• not abundant in nature.
• High power and high energy density.	• Transportation restriction.
• Relatively low self discharge.	• not mature, there is safety issues.
• Less maintenance required.	• Subjected to ageing effect i.e. during cold 40 % of charge may reduces.
• Large charge/discharge cycles.	• Limited Depth of Discharge (DoD).
• Round-trip efficiency is typically 80 - 90%.	• Needs thermal management.

3.5.3.2 Vanadium Redox Flow Battery (VRFB)

A Redox flow battery is an electrochemical energy storage device that converts chemical energy into electrical energy through reversible oxidation and reduction of working fluids [50]. The principle of storing energy in recirculating liquid electrolytes gives redox flow batteries merits of decoupled energy density and power generation capability. At present, even though redox flow batteries are not as commercially used like lithium-ion batteries, however in terms of system flexibility, quick response, and safety concerns, they have great advantages for large-scale applications and are expected to have higher commercial use in the future with more development into this technology.

In today's market, Vanadium Redox Flow Battery (VRFB) is the most developed redox flow battery type which is being used for grid-scale applications and most of the elements in it is similar to any other redox flow batteries. A major part of the battery is the chemical electrolytes that are stored in storage drums where one drum contains the chemical where Vanadium ion has a higher oxidation state, and another drum contains the chemical where Vanadium ion has a lower oxidation state. There are pipes and pumps required to circulate the electrolyte into a reaction chamber. The reaction chamber contains the positive and negative electrode and the separator, all required to convert the chemical energy into electrical energy.

- **Working principle of Vanadium Redox Flow Battery (VRFB):**

In a VRFB, vanadium salts are dissolved in concentrated solutions of sulfuric acid to form the electrolytes. The oxidation-reduction reactions in the two electrolytes gives rise to four states of vanadium with V^{2+}, V^{3+}, V^{4+} and V^{5+} oxidation states. Since the electrolytes contain the same element but with different oxidation state, mixing of the electrolytes is possible without any unstable situation. The positive electrolyte contains V^{4+} and V^{5+} species whereas the negative electrolyte contains the V^{2+} and V^{3+} species of vanadium. A typical maximum concentration of vanadium is 2M (2 moles per liter of solution) so that the vanadium ions remain soluble in the electrolyte in low temperatures and offer stability of the ions in high temperatures. In this way, this concentration offers operation of the VRFB over a wide range of temperatures [51].

During the charging process, the V^{4+} oxidizes in the positive electrolyte and becomes V^{5+} releasing an electron. This electron is transferred from the anode to the cathode through the external circuit which is then captured by V^{3+} and reduces to V^{2+} ion. The process is reversed during discharging where the V^{2+} is oxidized to V^{3+} in the negative electrolyte releasing electron to the cathode side which is then captured by V5+ ion and reduces to V^{4+} ion. Vanadium ions V^{4+} and V^{5+} are present in oxide form in the electrolyte as VO^{2+} and VO_2^+. The chemical reactions that take place in the cell are:

$$V^{2+} \leftrightarrows V^{3+} + V^{e-} \tag{3.7}$$

$$VO_2^+ + 2H^+ + e^- \leftrightarrows VO^{2+} + H_2O \tag{3.8}$$

where,
$\rightarrow$ represents the charge process.
$\leftarrow$ represents the discharge process.

- **Ageing of Vanadium Flow Batteries:**

The VRFB have longer life cycle compared to other traditional batteries and even much higher than Lithium-ion batteries. The process of ageing in VRFB is due to the continuous chemical reaction taking place in the reaction chamber. The separator used to separate the electrolytes in the chamber is selected in such a way that it only allows the movement of ions through it to maintain electroneutrality of the system. Various studies have shown that over time, the membrane degrades and crossing of ions from electrolyte to the other is observed which pollutes both the electrolytes and degrades the efficiency and lifetime of the battery [51]. Another problem with VRFB is that vanadium oxide tends to precipitate out from the electrolyte [52] causing a loss in the battery's capacity. One major degradation that occurs in the VRFB is the degradation of the electrodes. The graphite electrode tends to degrade over time with continuous chemical reaction taking place on its surface [52].

The main advantages and disadvantages Redox Flow Battery (RFB) are as follows:

Advantages	Disadvantages
• Expandable capacity through enlarging storage tanks.	• Cost is still high; not commercialized like Li-ion storage.
• Unlimited charge/discharge cycles.	• Relatively abundant material.
• Unlimited Depth of Discharge (DoD).	• Still not mature technology.
• High power density.	• Low energy density.
• Comparatively low environmental issue.	• Round-trip efficiency typically below 75 - 80 %.
• Quick and short response time.	• Enlarging tanks requires more aqueous electrolytes, makes battery heavier; thus, technology is suitable only for stationary application.

3.5.4 Life Cycle Cost (LCC) Assessment and Unit Price Calculation of ESS

In order to understand and quantitatively prove whether the ESS with different types of Energy Source is a viable and economical choice, a Life Cycle Cost (LCC) analysis is needed to be done. The LCC assessment is the process of estimating the total amount of money spent on a product throughout the course of its useful life [53]. All the costs are usually discounted and totalled to a present-day value known as net present value (NPV). In accordance to the international standard IEC 60300-3-3, the life cycle of a product should consist of the following six cost-causing phases: (1) Concept and Definition, (2) Design and Development, (3) Manufacturing, (4) Installation, (5) Operation and Maintenance and (6) Disposal [54]. These six cost-causing phases can be grouped in three components namely Investment Cost (I_k) which groups the phases 1 to 4, Operation and Maintenance Cost (OM_k) which corresponds to phase 5 and Disposing Cost (D_K) corresponds to phase 6. The lifetime of the product is determined by the number of years the product would be deemed useful and so the future costs should be discounted to consider the appropriate time value of money. The Life Cycle Cost can be formulated in terms of Net Present Value (NPV) as:

$$LCC = \sum_{k=0}^{n} \frac{I_k + OM_k + D_k}{(1+\rho)^k} \quad [\$] \tag{3.9}$$

where, n is the number of useful years of the product and ρ is the discount rate, normally taken to be 0.04.

The investment cost would be a one-time quantity and so would not recur over the years, but the cost of operation and maintenance would recur over the useful years of the product. In case of disposing of the product, since the energy storage source used

in our study can have second life application after its use in the grid-scale system, thus the cost occurring during disposing can be eliminated with the cash in flow through selling of the energy storage source.

So to proceed with the LCC assessment and the unit price calculations, the components involved for LCC of ESS and their prices are required. The components which would be included in the calculation are:

Initial Investment:

- Storage Block ($/MWh)
- Storage Balance of System ($/MWh)
- Power Equipment ($/MW)
- Controls and Communications ($/MW)
- System Integration ($/MWh)
- Engineering, Procurement and Construction ($/MWh)
- Project Development ($/MWh)
- Grid integration ($/MW)

Operation and Maintenance:

- Fixed Operation and Maintenance Cost ($/MW - yr)
- Variable Operation and Maintenance Cost ($/MWh)

The prices of the components were obtained from [75] in which the prices of ESS systems of 1MW, 10MW and 100MW respectively were specified. The report also contained the prices from the year 2020 and the estimated prices for the year 2030. The number of life cycles for the different energy sources has also been specified and so if the number of times the ESS were to be activated annually can be calculated, then the useful lifetime in years of the ESS could also be calculated.

According to SvK, the system frequency is within the FCR-D activation window for 2.31% of the year (accounting for both FCR-D upwards and FCR-D downwards) [76]. By assuming an average activation duration of FCR-D from ESS to be 15 minutes, the number of activations annually can be calculated as:

$$No.\ of Annual\ Activation = \frac{\frac{2.31}{100} \times 365 \times 24 \times 60}{15} \tag{3.10}$$

By using the number of annual activations, the lifetime of the ESS can be calculated:

$$Life - time\ (Years) = \frac{No.\ of\ life\ cycles}{No.\ of\ Annual\ Activation} \tag{3.11}$$

By using the lifetime, the total life cycle cost were calculated for the three sizes of ESS (1MW/0.25MWh, 10MW/2.5MWh and 100MW/25MWh) as well as for the year 2020 and 2030. It is to be noted that since the average activation time has been taken to be 15 minutes, so the energy capacity of the ESS has been sized according to the assumption.

In order to calculate the price of FCR-D from ESS, we need to estimate the number of times the ESS would be activated in its lifetime and so by dividing the total

life cycle cost with the number of times the ESS would activated would give us an average price for each activation which we will assume to be the price of FCR-D support from the ESS. Since the prices for three sizes of ESS were calculated, the price of each unit MW support from the ESS can be easily calculated. So, the unit price variation would be:

$$Unit\ Price\ of\ ESS(1 \approx 9.9MW) = \frac{Price\ of\ 1MW/0.25MWh}{1}\ \$ \tag{3.12}$$

$$Unit\ Price\ of\ ESS(10 \approx 99MW) = \frac{Price\ of\ 10MW/2.5MWh}{10}\ \$ \tag{3.13}$$

$$Unit\ Price\ of\ ESS(100MW \approx and\ above) = \frac{Price\ of\ 100MW/25MWh}{100}\ \$ \tag{3.14}$$

The prices can then be converted to Euros according to the exchange rate.

4

Study Method and Modelling for Dynamic Simulation Studies

4.1 Study Method

The thesis would be approached based on the knowledge and understanding gained through literature review of frequency instability with higher renewable energy penetration into the electrical grid. A modified Nordic-32 grid would be setup with the principle of reducing generated power from thermal power stations and substituting with the power generated from renewable energy power plants. The amount of renewable energy penetration into the grid would be increased in three steps (10%, 20% and 30% respectively) and the frequency response would be observed for a common N-1 contingency criteria disturbance. The primary frequency regulation scheme would be changed from a governor droop controlled model, already present in the Nordic-32 grid as default, to a scheme defined in the Technical Requirements for FCR-D documentation [21]. A common reference point of frequency deviation would be kept to illustrate the difference in power requirement from the primary frequency regulation for different scenarios of modified Nordic-32 grid and their renewable energy penetration proportions. Finally, the results from the simulations would be used in conjunction with the prices of different energy storage solutions as a source for FCR-D support as well as the price of traditional FCR-D support to numerically calculate the estimated overall cost of FCR-D support with a combination of the two types of support sources (Traditional FCR-D with Lithium-ion battery-based ESS and Traditional FCR-D with Vanadium Redox Flow battery-based ESS). The flow charts on the methods used can be illustrated in Figures 4.1 and 4.2 below:

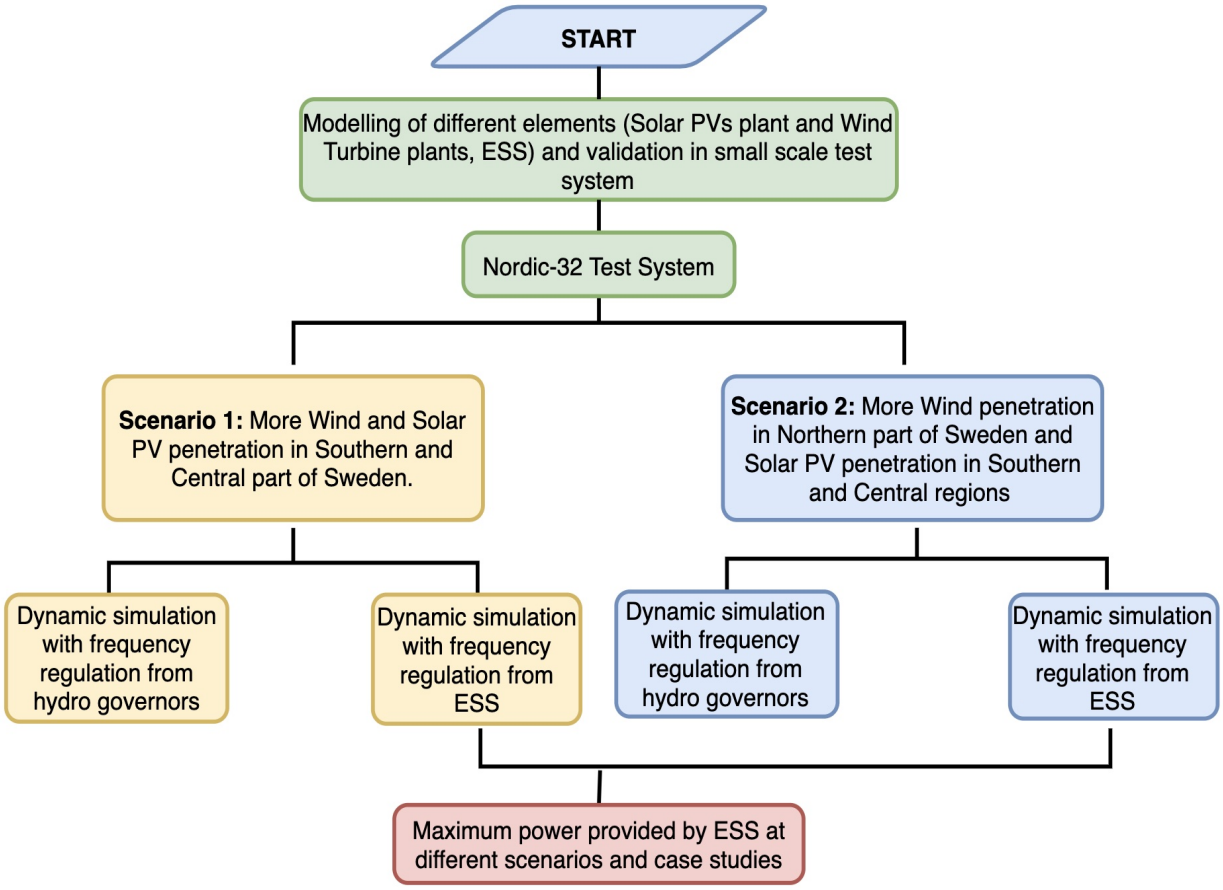

Figure 4.1: Dynamic study process.

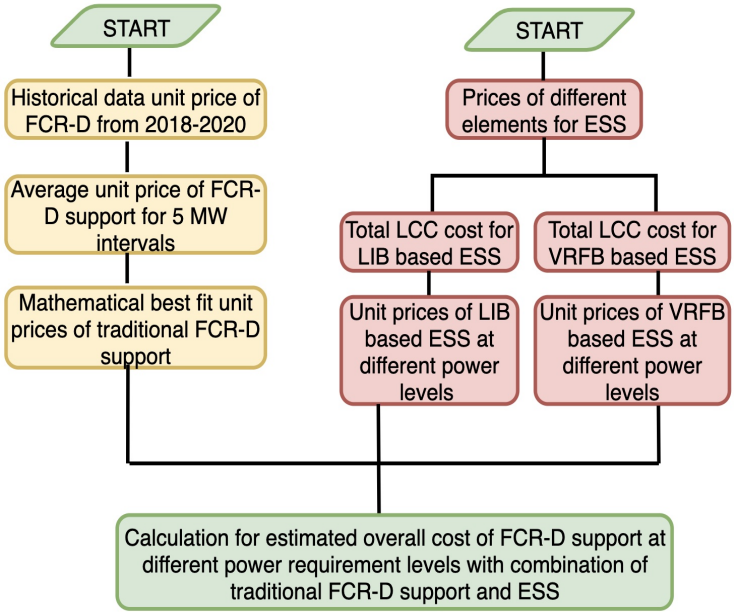

Figure 4.2: Process of cost calculations for FCR-D support.

4.2 Modelling of different elements for Dynamic Simulation Studies

4.2.1 Introduction to Nordic 32 Test System

The Swedish Transmission Grid or National Grid is composed of approximately 17,000 km of power lines, about 200 substations and switching stations and 16 connections to other countries [55]. SvK is responsible since 1992 for the maintenance and development of the grid. The complete Swedish grid is divided into four parts SE1, SE2, SE3 and SE4. The main generation for the grid comes from the northern part of the country and a lot of consumption is in the southern part of the country. For this reason, there are eight 400 kV transmission lines between SE2 and SE3 that connect the north side of the grid to the southern part. The lines are also equipped with series compensation to increase stability and enhance transfer capacity of the lines [56].

The Nordic 32 test system is based on the Swedish transmission grid from 1995 [57]. The test system is designed to simulate large transfers of electrical power from the Northern part of the grid where the hydro power stations are located, to the Central and Southern part where most of the loads are located. The complete test system is divided into four parts:

1. **'North'** where majority of hydro power generators are located with some load connections as well.
2. **'Central'** where majority of thermal power generators and loads are situated.
3. **'South'** where some of the thermal power generators and loads are located.
4. **'Equiv.'** is the interconnection between Sweden and the neighboring countries simulating the import/export of power from the grid.

The Nordic 32 test system has a nominal frequency of 50 Hz with a total of 74 busses, 102 branches, 20 generators (all with step-up transformers and over-excitation limiters), 22 loads in the distribution level [58]. Figure 4.3 represents the single line diagram of the Nordic-32 test system. Table 4.1 below shows the active power generation and consumption in the Nordic 32 test system.

Table 4.1: The table below shows the apparent power and generated active power of the generators in the Nordic-32 grid [58].

Area	Power generated [MW]	Power consumed [MW]
North	4628.5	1180.0
Central	2850.0	6190.0
South	1590.0	1390.0
Equiv.	2437.4	2300.0
Total	11505.9	11060.0

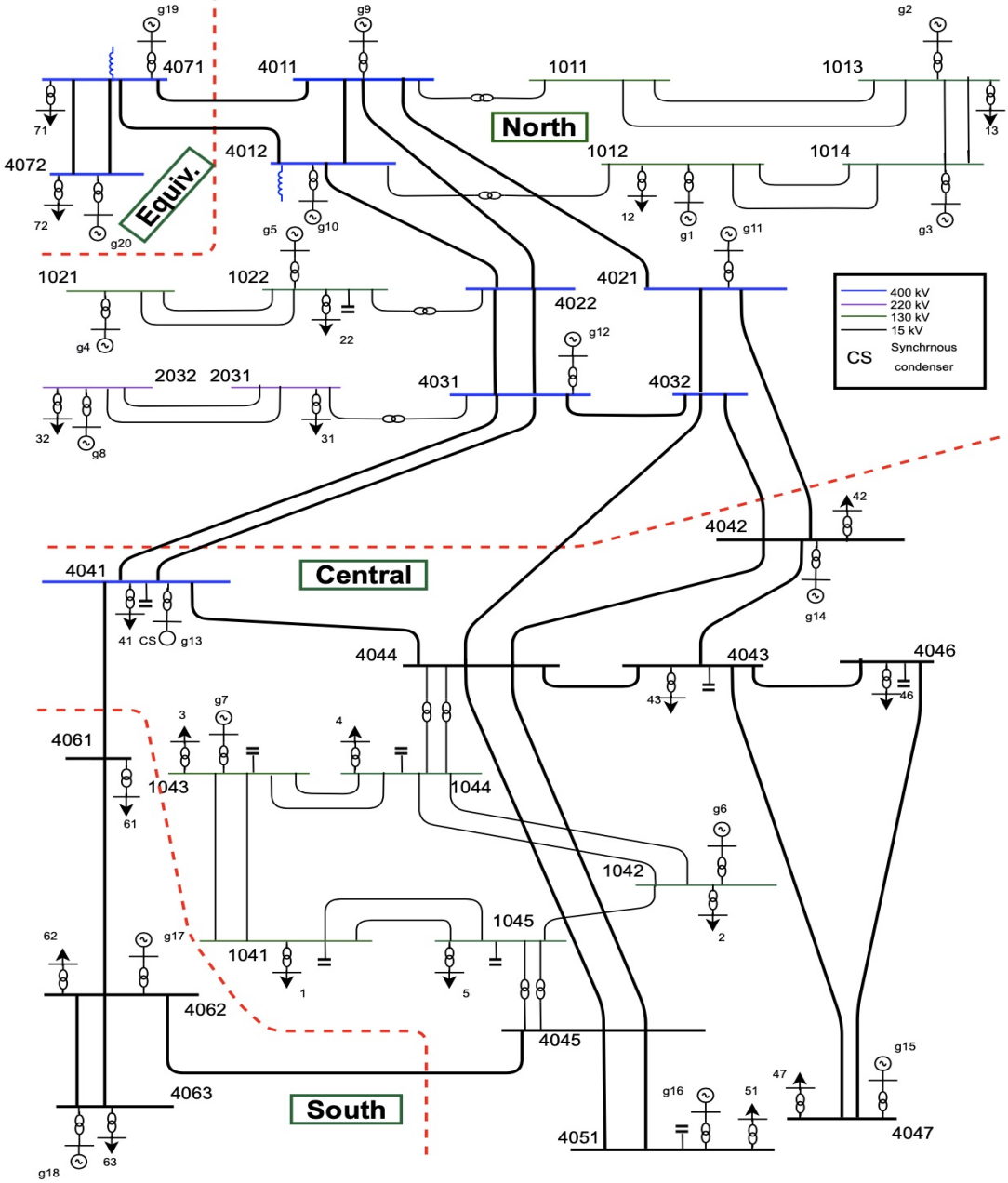

Figure 4.3: Nordic-32 Test System.

4.2.1.1 Generator Model

The Nordic 32 test system contains a total of 20 generators of which 12 are hydro turbines with salient-pole generator, 7 are thermal with round rotor generator and 1 generator with salient-pole acts as a synchronous condenser, providing reactive power only. Table 4.2 shows the lists of generators with their apparent and active power generation and Table 4.3 shows the lists of the machine data of the generators in Nordic-32 test system.

Gener.	S_{norm} (MVA)	P_{norm} (MW)
$g1$	800.0	760.0
$g2$	600.0	570.0
$g3$	700.0	665.0
$g4$	600.0	570.0
$g5$	250.0	237.5
$g6$	400.0	360.0
$g7$	200.0	180.0
$g8$	850.0	807.5
$g9$	1000.0	950.0
$g10$	800.0	760.0
$g11$	300.0	285.0
$g12$	350.0	332.5
$g13$	300.0	0.0
$g14$	700.0	630.0
$g15$	1200.0	1080.0
$g16$	700.0	630.0
$g17$	600.0	540.0
$g18$	1200.0	1080.0
$g19$	500.0	475.0
$g20$	4500.0	4275.0

Table 4.2: Represents the participating generators in Nordic-32 and their Active and Apparent power [58]).

	Round rotor	Salient pole	Salient-pole
	$g6, g7, g14, g15$ $g16, g17, g18$	$g1, g2, g3, g4$ $g5, g8, g9, g10$ $g11, g12, g19, g20$	$g13$
$X_d(pu)$	2.20	1.10	1.55
$X_q(pu)$	2.00	0.70	1.00
$X'_d(pu)$	0.30	0.25	0.30
$X'_q(pu)$	0.40	0.00	0.00
$X''_d(pu)$	0.20	0.20	0.20
$X''_q(pu)$	0.20	0.20	0.20
$T'_{do}(s)$	7.00	5.00	7.00
$T'_{qo}(s)$	1.50	0.00	0.00
$T''_{do}(s)$	0.05	0.05	0.05
$T''_{qo}(s)$	0.05	0.10	0.10
$H(s)$	6.00	3.00	2.00
$i_{fd}^{rated}(pu)$	2.9160	1.8087	2.8170

Table 4.3: Represents machine data of generators in Nordic-32 (adapted from [58]).

All the generators have over-excitation limiter model, voltage regulator model, excitation model and power system stabilizer model built into their dynamic models. However, our main concern is with the turbine model and the speed governor model of the hydro turbines which are responsible for the frequency stability of the Nordic 32 test system in case of disturbance.

- **Turbine model data:**

In case of the thermal plants, a constant mechanical torque is assumed. For the case of hydro turbines, the turbines are represented by a lossless model shown in the figure below. The water time constant is taken as 1 second. In the model, z is the gate opening, q is the water flow, H is the head, P_m is the mechanical power and P_m the mechanical torque, all in per unit of nominal base P_{norm}. ω is the rotor speed in per unit as well.

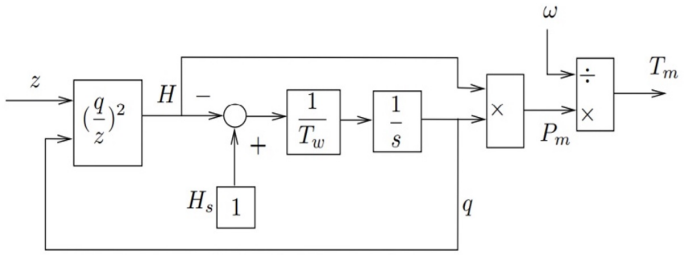

Figure 4.4: Hydro Turbine Model [58].

- **Speed governor model and data:**

The speed governor model contains a simple power measurement proportional and integral (PI) control and a servomotor. P is the active power, P^0 is the power set point, z is the gate opening and ω the rotor speed. The servomotor is modelled as a first order system having a time constant of 0.2 seconds. The permanent speed droop σ varies from one machine to another where the value is 0.08 for generator 19 and 20 and 0.04 for the other hydro turbines [58].

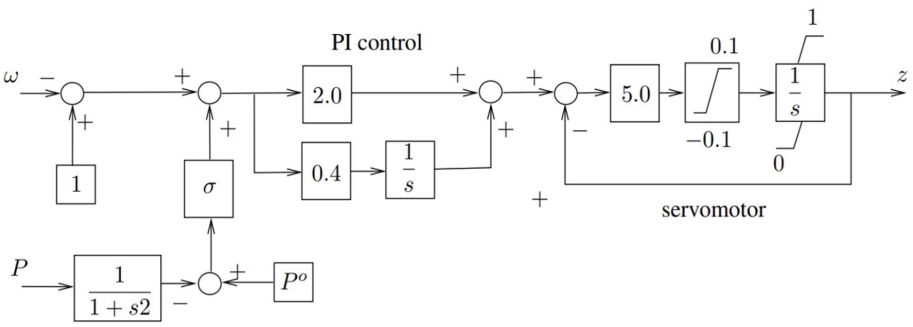

Figure 4.5: Speed governor Model [58].

4.2.1.2 Load Model

The loads in the Nordic 32 test system are connected to the 20 kV buses. They have an exponential model:

$$P = P_o \left(\frac{V}{V_o}\right)^{\alpha}; Q = Q_o \left(\frac{V}{V_o}\right)^{\beta} \tag{4.1}$$

with $\alpha = 1.0$ (constant current) $\beta = 2.0$ (constant impedance), respectively and V0 is set to the initial voltage of the bus before dynamic simulation [58].

4.2.2 Modelling of Wind Turbines and Solar PV plants

4.2.2.1 Modelling and Integration of Wind Turbines

The modern wind turbines which are connected to the grid are all full converter type wind turbines. The full converter wind turbine (FCWT) employs a permanent magnet alternator (PMA). This technology has a number of significant advantages; it effectively decouples the generator from the grid, improving fault response and allows the turbine to operate over a wide speed range, leading to improved power extraction from the wind. However, since the generator is decoupled from the grid, the rotating turbine does not contribute any inertial response during any disturbance in the grid.

There are many wind turbine models that are already present in the PSS®E software. However, we have chosen to perform our dynamic simulation studies using a Type-4 wind turbine model. This is because Type-4 wind turbine models are designed to simulate the behavior of a FCWT during dynamic simulation. The dynamic model values of the Type-4 wind turbine are a reference from a GE 2.5MW Wind Turbine [59].

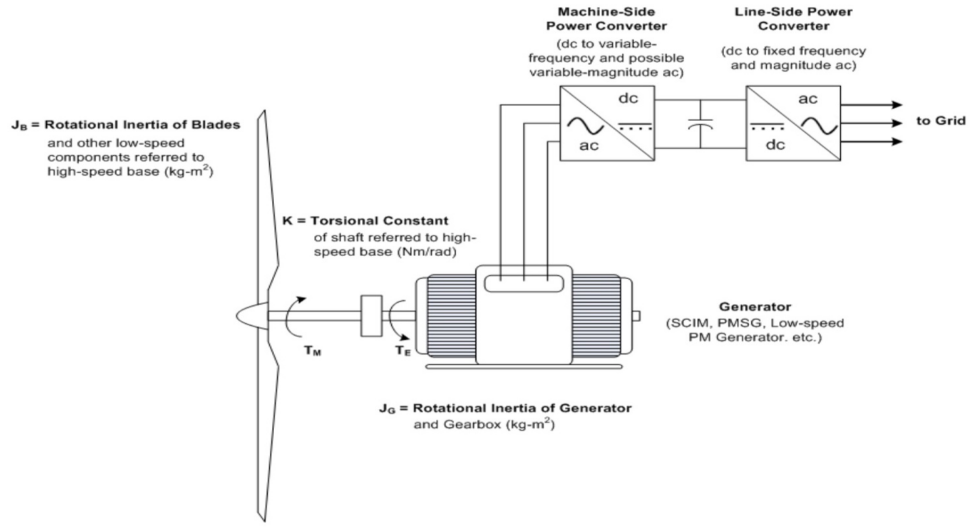

Figure 4.6: A WT4 generator connected to electrical grid via full power converter [59].

- **Power Flow Setup:**

A generic Type-4 wind turbine is disconnected from the electrical grid by the full power converter as seen in Figure 4.6. During power flow, the full power converter can be treated as the generator related to the wind machine category of the existing generator record of the Power Flow Raw Data File [59]. The suggestion on aggregation of wind farm model is presented in [59]. However, the method involved in aggregation of wind farm is discussed further in Section 4.2.2.3.

- **Dynamic Setup:**

A generic Type-4 Wind Turbine Model in PSS®E have the two following modules:

1. WT4G1 : Power Converter/Generator module.
2. WT4E1 : Electrical Control module.

The dynamic data for the two modules are taken from the PSS®E Application Guide [59] with reference to a GE 2.5 MW wind turbine. For further details, explanation can be found in [59]. The dynamic data for the wind turbine used during the simulation studies has been attached in Appendix A.

4.2.2.2 Modelling and Integration of Solar PV plants

The Solar PV plants and farms used now-a-days are all full converter type, meaning, the energy extracted by the solar PVs from the solar energy is converted from DC to AC with the help of the converter which then transfers the power to the grid via a step-up transformer. The converter controls the complete electrical generation from the plant which includes both active and reactive power. The solar PV model in PSS®E used for dynamic simulations was developed to simulate the performance of a PV plant connected to the grid via a power converter. The model is largely based on the Generic Type-4 wind turbine model with the added ability to simulate changes in the output due to changes in solar irradiation profile [59].

- **Power Flow Setup:**

Just like the Type-4 wind turbine model, the solar PV is also decoupled from electrical grid by the full power converter. The suggestion on aggregation of solar PV model is presented in [59]. However, the method involved in aggregation of solar PV is discussed further in Section 4.2.2.3.

- **Dynamic setup:**

The solar PV model in PSS®E have the four following modules:

1. PVGU1 : Power Converter/Generator module.
2. PVEU1 : Electrical Control module.
3. PANELU1 : Linearized Model of a Panel's output curve.
4. IRRADU1 : Linearized Solar Irradiance profile.

The dynamic data for above module in order to perform simulation is taken from the PSS®E application guide [59]. For further details, explanation can be found in [59]. The dynamic data of the solar PVs used during the simulation study in this thesis has been attached in appendix A.

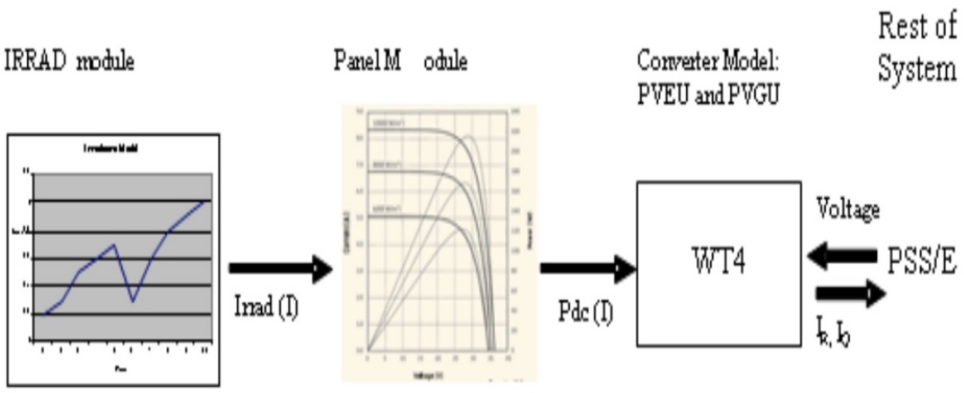

Figure 4.7: Solar PV model connectivity diagram, showing interactions between module [59].

4.2.2.3 Aggregated models of Wind Turbines and Solar PVs

In a real scenario, utility scale of Wind Power Plant (WPP) and Solar Photo-Voltaic Power Plant (SPVPP) consists of large number of identical wind turbines and solar PV modules. Considering single units while studying power system stability may increase complexity and cause prolong simulation time. Therefore, in order to show proper and accurate dynamic simulation results during case study with a grid consisting of wind turbines and solar PV modules, a proper simplification of large number of wind turbines and solar PVs calls for a novel model i.e. an aggregated model.
For dynamic stability study of power system, an appropriate electrical and mechanical model of solar PVs and wind turbines is necessary. The aggregation method for fixed-speed wind farm is discussed in [60]. However, in this thesis, Type 4 wind turbine (Variable-speed Full Converter wind turbine (FCWT)) model is emphasized for aggregation of WPP and SPVPP.

Aggregation method

For identical machines comprising of large number of wind turbines and solar PVs, single machine aggregated model of WPP and SPVPP can be determined by simply multiplying rated Type 4 wind turbine power with number of turbine units. Hence, equivalent MVA rating of generator can be represented as-

$$S_{eqv.} = n \cdot S_r \tag{4.2}$$

where,
$S_{eqv.}$= Equivalent MVA rating of generator.
n= Number of identical turbine units.
S_r= MVA rating of single type 4 wind turbine.

In addition, in order to keep the bus voltage within the nominal rated value of each bus connecting the WPP and SPVPP units, maintaining the equivalent limit for Q_{max}/Q_{min} of reactive power (MVAr) is of great importance. Hence, equivalent reactive power limit is represented as-

$$Q_{eqv.}^{max} = [n \cdot Q_{max}] \tag{4.3}$$

$$Q_{eqv.}^{min} = -\left[n \cdot Q_{min}\right] \tag{4.4}$$

Apart from these, other electrical components such as compensating capacitors and unit transformer modelling is also significantly important.

4.2.3 Modelling of ESS

The Energy Storage System (ESS) that is to be implemented into the electrical grid for dynamic studies has no generic model in the PSS®E Model Library. The only suitable model the library contains is for a Battery Energy Storage System developed by the Electric Power Research Institute (EPRI) named 'CBEST'. The CBEST model has been used in many research studies [61], [62], [63], [64].

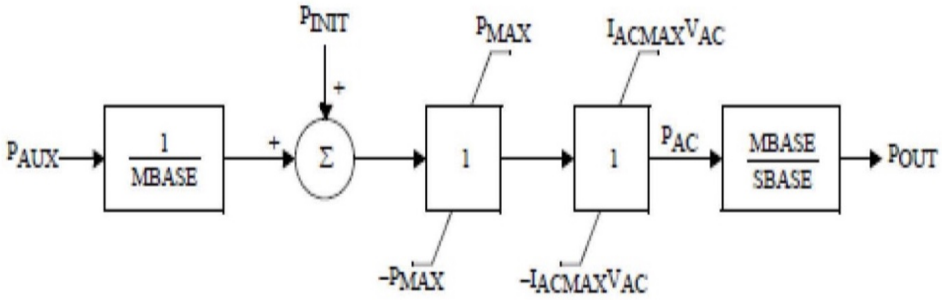

Figure 4.8: Block diagram of CBEST model [81].

In order to integrate the CBEST model as our ESS, we need to control the value of P_{AUX} in order to condition the output according to our requirements. For this reason, the dynamic simulations of PSS®E has been run through Python programming script using various Application Programming Interfaces (APIs) present in the PSS®E API Documentation [65]. By doing so, the value of P_{AUX} can be conditioned using various equations containing system frequency as variable in the Python script and the result will be sent back to the CBEST model as input. The CBEST model will then process this input and provide the necessary output.

For this thesis study, the ESS model would be used to only provide FCR-D support to the electrical grid and would need to satisfy the requirements specified by the SvK's technical requirements documentation [21]. As stated in the documentation, the ESS should be able to provide active power as a linear function to the change in the system frequency with maximum power generated when the frequency is equal to or below 49.5 Hz and a maximum power consumed when the frequency is equal to or above 50.5 Hz. The ESS should not activate within the frequency band of $49.9Hz \leq f_0 \leq 50.1Hz$. This characterization is called Droop Control of the ESS which has also been shown in Figure 4.9. The dynamic data for the CBEST model used as ESS during the simulation studies has been attached in Appendix A.

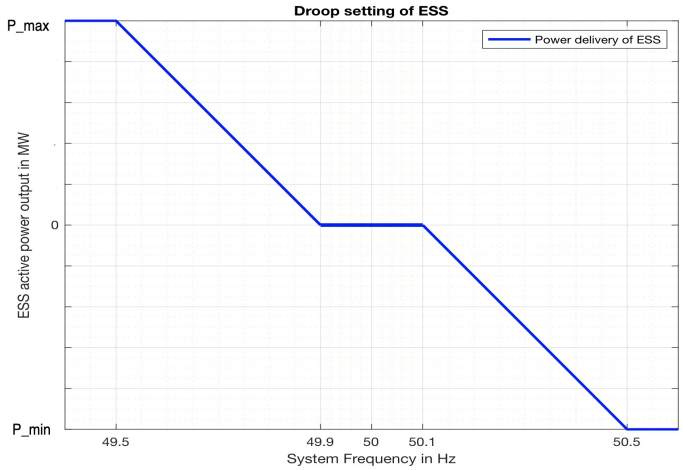

Figure 4.9: Droop setting of ESS.

4.2.4 Validation of dynamic models in small scale network

The models in the previous section are needed to be integrated into an electrical network in order to verify that they are working properly. For this reason, a small scale network is used such that any troubleshooting necessary would be faster to detect and easier to perform. The Kundurs Model was chosen as the small scale network since it contains all the necessary components that are also present in the Nordic-32 test system. However, some adjustments to the base form of the Kundurs model had to be done to accommodate the wind turbine Model, the solar PV model and the ESS model. The adjusted Kundurs model is shown in Figure 4.10.

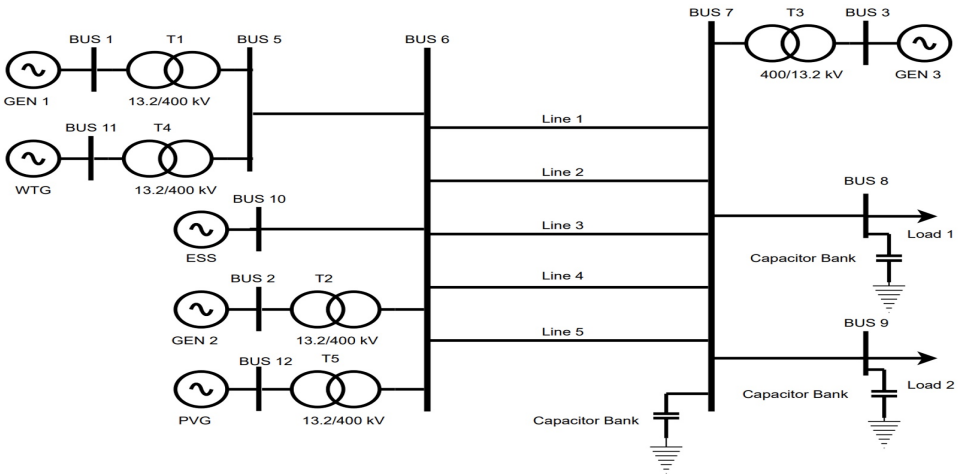

Figure 4.10: Modelling of Wind and Solar PV in conjunction with Hydro power plant (Kundurs' Model).

The modified Kundurs model is composed of a total of 6 Generators where, GEN 1, GEN 2 and GEN 3 are modelled as hydro turbines, WTG is modelled as a Type-4 wind turbine, PVG is modelled as a solar PV plant and ESS is modelled as the energy storage system providing the FCR-D support for the network.

It is to be noted that the governor droop control of the hydro turbines used in this network is also activated as well. So in case of any disturbance or a change in frequency would cause a change in the active power delivery by the hydro turbines according to the governor droop control as well as the FCR-D support from the ESS would also be activated. This is only done to test the proper functionality of the generators governor models and the FCR-D support of ESS.

In order to observe the frequency response to an N-1 contingency criteria, a specific disturbance has be to selected and kept constant throughout all the simulations. For the small scale network, GEN 3 was chosen, meaning that GEN 3 would be tripped from the electric grid and the dynamic frequency response as well as the power delivery response from the ESS would be observed. Figure 4.11 shows the change in active power generated by the ESS with change in system frequency. As can be seen with a maximum power of 20MW, the ESS is able to ramp up and change its active power according to the change in frequency. According to SvK's technical specification requirements, the behavior of the ESS is compliant with all the requirements for FCR-D support.

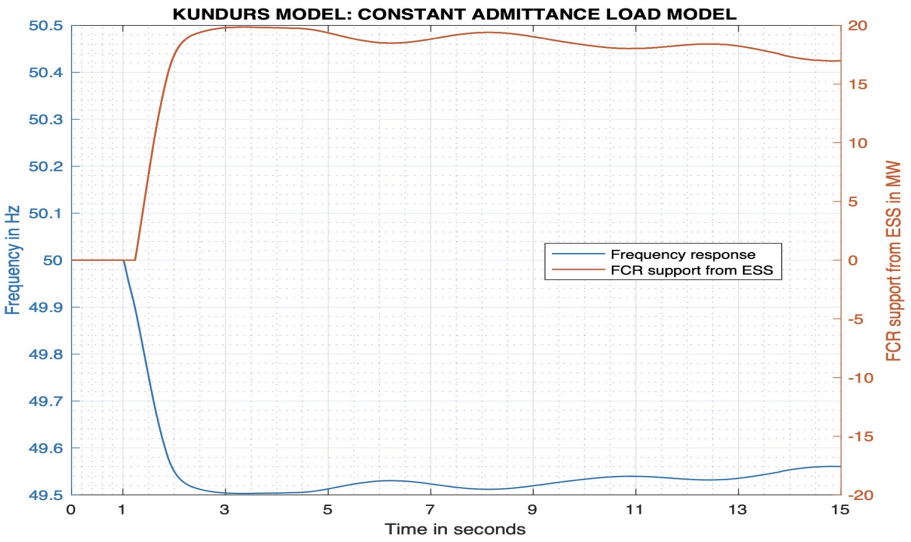

Figure 4.11: Kundurs model: Frequency response and active power support from ESS.

4.2.4.1 Performing Dynamic Simulation with Renewable Energy Penetration

The test network would now be used for further studies with different penetration levels of renewable energy and observing the effect to the network's frequency response with the same N-1 contingency criteria. The active power generated by the hydro turbines are reduced in steps and the active power generated by the renewable energy power plant connected to the same bus are increased in the same proportion. The percentage of renewable energy penetration is calculated according to the equation below:

$$\%\ RE\ Penetration = \left(\frac{Installed\ capacity\ of\ RE\ based\ power\ plants}{Total\ system\ installed\ capacity} \right) * 100 \tag{4.5}$$

For the first test case study, both the renewable energy power plants were modelled as wind turbines. Figure 4.12 shows the frequency nadir of the network with different penetration of wind energy into the system.

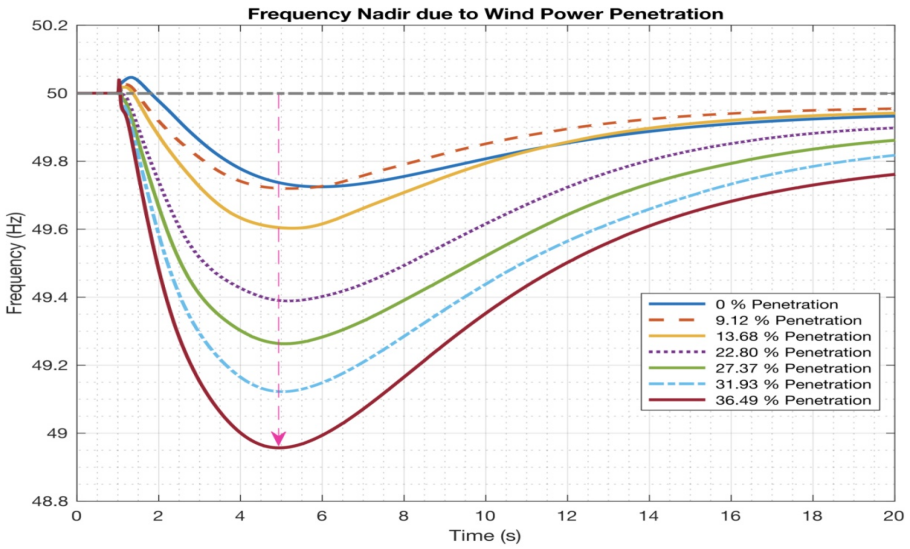

Figure 4.12: Frequency Nadir due to Wind Power Penetration (simulated in PSS ®E).

With wind energy penetration, the maximum penetration achievable with this test model without the use of FCR-D from ESS was around 36.48 percent, with a maximum frequency deviation of -1.043 Hz using only the governor droop control of the hydro turbines. Load shedding has already begun in this deviation, so allowing further penetration will result in the failure of the protection system and the machine being rendered inoperable. The FCR-D support from ESS was activated for the cases where the frequency deviation was higher than -0.5 Hz such that the FCR-D power requirements were changed to bring the minimum frequency dip to within 49.5 Hz. This method was used to show the change in power requirement for the FCR-D support from ESS with varying renewable energy penetration keeping a reference point which in this case was the minimum frequency of 49.5 Hz. Table 4.4 shows the variation of maximum power of the FCR-D used with variation in renewable energy penetration from wind energy.

Table 4.4: Frequency deviation due to Wind power penetration for the case with or without FCR-D support.

Wind Power	**Without FCR-D support**	**With FCR-D support**			
Penetration (%)	Maximum Frequency Deviation (Hz)	Maximum Frequency Deviation (Hz)	Power demand (MW)	Energy supplied (kWh)	Settled Frequency (Hz)
0	-0.275	-0.275	0	0	49.725
9.12	-0.282	-0.282	0	0	49.718
13.68	-0.397	-0.397	0	0	49.603
22.80	-0.611	-0.495	48	142.535	49.505
27.37	-0.737	-0.507	85	306.526	49.492
31.93	-0.878	-0.500	128	511.406	49.500
36.49	-1.043	-0.505	170	717.617	49.49

For the second test case study, both the renewable energy power plants were modelled as solar PV plants. Figure 4.13 shows the frequency nadir of the network with different penetration of Solar PVs into the system.

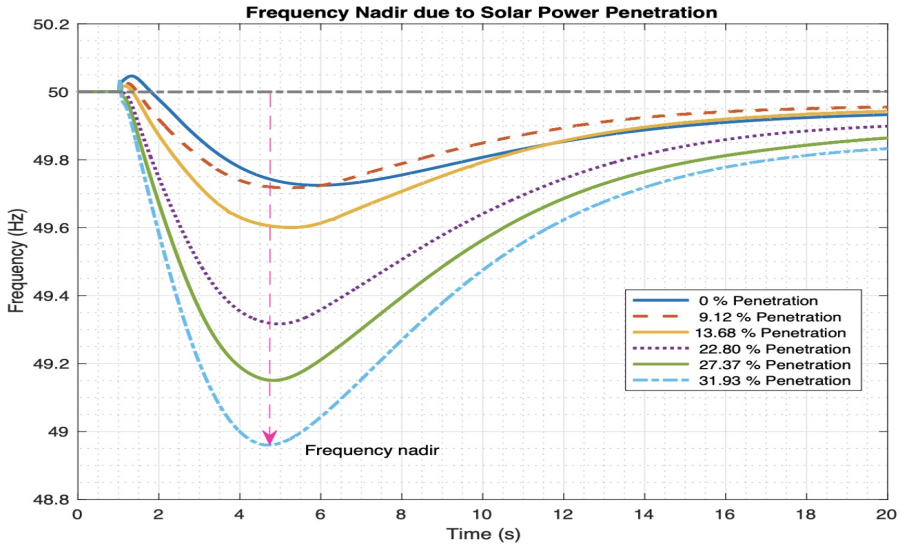

Figure 4.13: Frequency Nadir due to Solar Power Penetration (simulated in PSS®E).

With solar PV penetration, the maximum penetration achievable with this test model without the use of FCR-D from ESS was around 31.93 percent, with a maximum frequency deviation of -1.040 Hz using only the governor droop control of the hydro turbines.As previously done, the same process is used to find out the power requirements from the FCR-D support provided by the ESS. Table 4.5 shows the variation of maximum power of the FCR-D used with variation in renewable energy penetration from Solar PVs.

Table 4.5: Frequency deviation due to Solar power penetration for the case with or without FCR-D support.

Solar Power	**Without FCR-D support**	**With FCR-D support**			
Penetration (%)	Maximum Frequency Deviation (Hz)	Maximum Frequency Deviation (Hz)	Power demand (MW)	Energy supplied (kWh)	Settled Frequency (Hz)
0	-0.275	-0.275	0	0	49.725
9.12	-0.283	-0.283	0	0	49.716
13.68	-0.399	-0.399	0	0	49.600
22.80	-0.683	-0.503	81	226.998	49.500
27.37	-0.849	-0.500	145	464.436	49.500
31.93	-1.040	-0.505	200	704.039	49.500

For the third and final test case study, the renewable energy power plants were modelled as solar PV and wind turbine, i.e. WTG generator was modelled as a wind turbine and PVG generator was modelled as a solar PV plant. Figure 4.14 shows the frequency nadir of the network with different renewable energy penetration from both solar PV and wind turbine into the system.

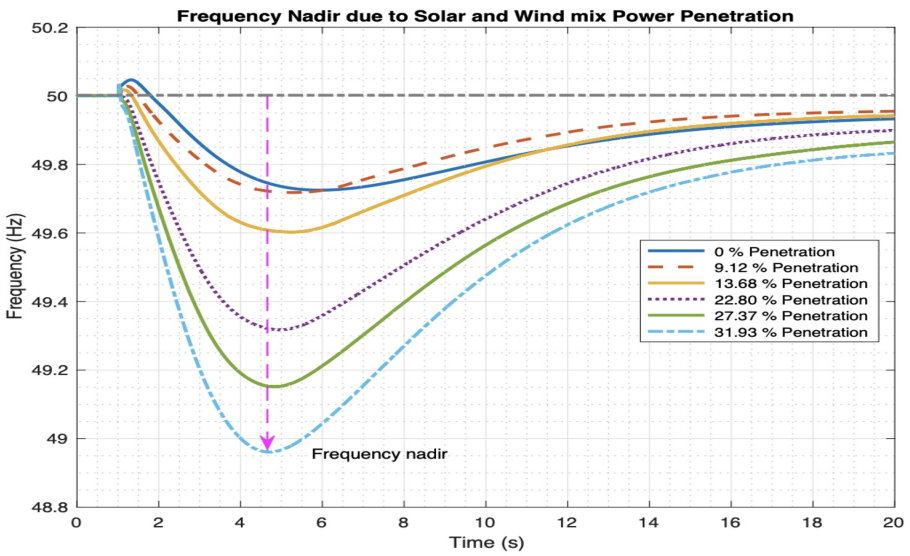

Figure 4.14: Frequency Nadir due to Solar and Wind mix Power Penetration (simulated in PSS®E).

With solar and wind energy penetration, the maximum penetration achievable with this test model without the use of FCR-D from ESS was around 31.93 percent, with a maximum frequency deviation of -1.039 Hz using only the governor droop control of the hydro turbines. As previously done, the same process was used to find out the power requirements from the FCR-D support provided by the ESS. Table 4.6 shows

the variation of maximum power of the FCR-D used with variation in renewable energy penetration from solar PV and wind turbine.

Table 4.6: Frequency deviation due to Solar + Wind mix power penetration for the case with or without FCR-D support.

Solar + Wind Power	**Without FCR-D support**	**With FCR-D support**			
Penetration (%)	Maximum Frequency Deviation (Hz)	Maximum Frequency Deviation (Hz)	Power demand (MW)	Energy supplied (kWh)	Settled Frequency (Hz)
0	-0.275	-0.275	0	0	49.725
9.12	-0.282	-0.282	0	0	49.718
13.68	-0.397	-0.397	0	0	49.603
22.80	-0.682	-0.501	82	228.570	49.500
27.37	-0.848	-0.500	145	464.436	49.500
31.93	-1.039	-0.504	200	702.789	49.500

The results from the three test case studies were also presented in graphical plots in which Figure 4.15 represents the variation of energy provided by the FCR-D support from the ESS with change in renewable energy penetration for the three test cases, Figure 4.16 represents the variation of Maximum power provided by the FCR-D support from the ESS with change in renewable energy penetration for the three test cases and Figure 4.17 represents the variation of frequency nadir of the network with change in renewable energy penetration for the three test cases respectively.

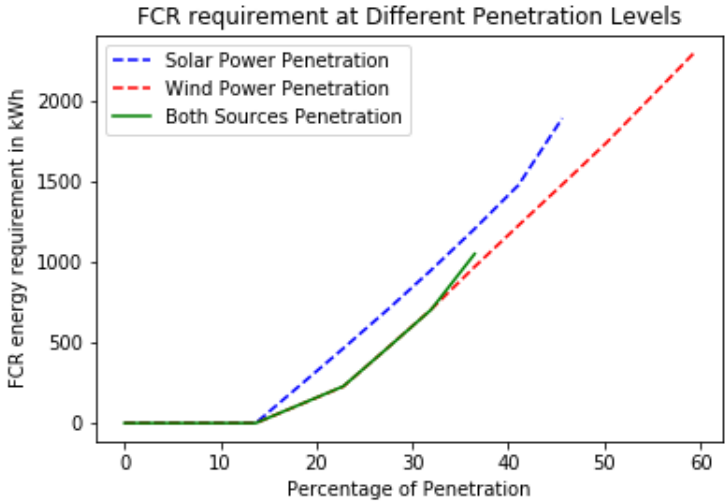

Figure 4.15: FCR requirement at Different Penetration Level, kWh.

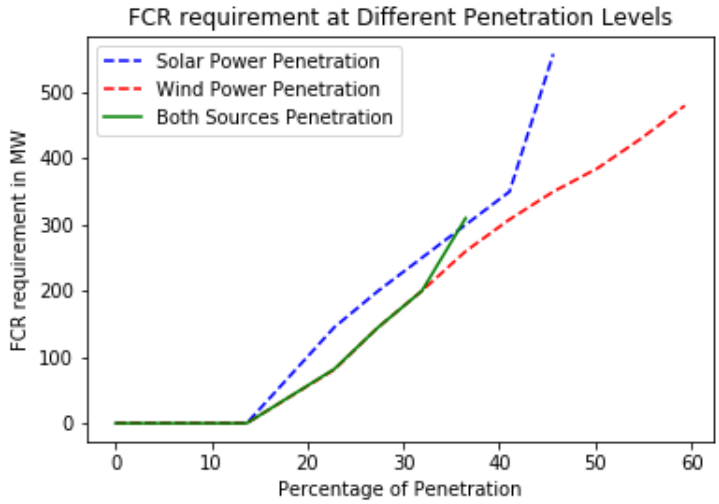

Figure 4.16: FCR requirement at Different Penetration Level, MW.

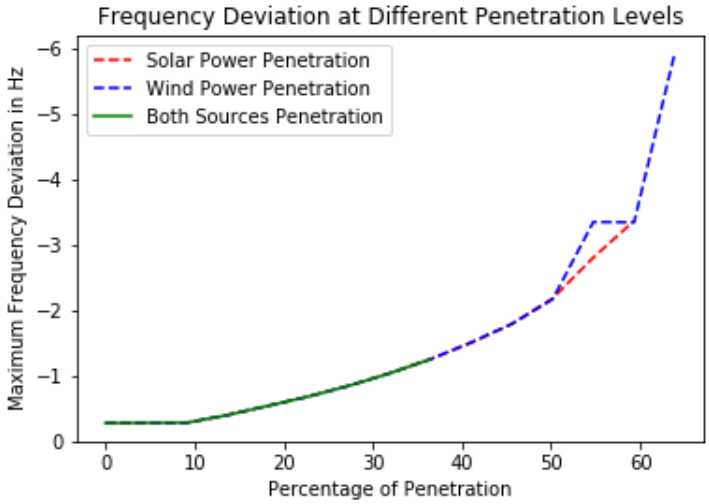

Figure 4.17: Frequency Deviation at Different Penetration Level.

5

Description of Case Studies and Renewable Scenarios

5.1 Philosophy of Simulation Scenarios and Case Studies

World is witnessing very fast energy transition in order to reduce the CO_2 emissions. Sweden as a part of the Nordic countries is also aiming to have 100 % renewable energy by 2040 with increasing wind and some fraction of solar PV penetrating into the national grid. Swedish TSO, SvK prepares a development plan every year in order to move towards and fulfil this ambitious target. Sweden has a lot of wind energy potential in Northern as well as in the Southern (offshore) sites. Therefore, to provide a practical representation of the Swedish grid with higher renewable energy penetration, some scenarios has been prepared within the Nordic-32 test grid following the System Development Plan [7], Network Development Plan [8] and Nordic Development Plan [9].

5.1.1 Achieving Renewable Energy Penetration in the Nordic-32 Test System

In order to perform representative simulation studies, some assumptions has been made within the Nordic-32 test grid that all the hydro power plant situated mostly in Northern and Equivalent area will remain unchanged. However, all the thermal power plants situated in Southern and Central location will be replaced by wind and solar PV plants as per their capacity factor. This is a good assumption to make since by doing so, the carbon footprint of the grid would be reduced and it corresponds to the development plans of the Swedish TSO. As stated in [66], the capacity factor for solar PV in Sweden accounts to approximately 10 % and in case of wind turbines, the capacity factor increases to approximately 28 % as per Svensk Vindenergi report [67]. However, the wind capacity factor can be increased to 40 % with building of offshore wind turbines in Swedish waters which has been stated by the Baltic Sea Region Energy Co-operation (BASREC) [68]. We also assumed that the total amount of electrical energy produced by the solar PV and the wind turbines annually would be equal. So in order to maintain it, the ratio of capacity factor 1:4 (Solar PV capacity $= 4 \times$ Wind capacity) and hence the installed capacity ratio between them has been maintain during simulations in the modified Nordic-32 test grid.

5.1.2 Dynamic Simulation Process

The main objective of the simulation study was to observe the frequency response of the modified Nordic-32 test system with change in renewable energy penetration under a disturbance of N-1 contingency criteria. During the dynamic simulation, the system was ran in steady state for 1 second before a disturbance was introduced into the system in the form of Generator G10 tripping. According to [58], the hydro turbines present in the Nordic-32 test system, all have governor droop control for frequency stabilization. However, for our studies, the governor droop control would be turned off when the FCR-D support from the ESS would be enabled and vice versa. In a real scenario, the primary frequency regulation supports FCR-N and FCR-D would both be activated when the frequency is lower than 49.9 Hz and the secondary frequency regulation aFRR would also be activated shortly after them to hold back the frequency from dropping any further. Since the simulation study is only focusing on FCR-D support by the ESS, the power from the ESS would be able to slow down the frequency deviation but would not be sufficient enough to keep the frequency from falling further. For this reason, a reference point has been selected such that the system frequency falls to but not below 49.4 Hz at 30 seconds of simulation with only FCR-D support from ESS. The ESS models have been placed in the same busses as that of the hydro turbines in order to keep the location of primary frequency regulation support unchanged throughout the studies. The simulations were also performed with different loading profiles provided by [69] to observe and gain a better understanding of the dynamic behavior of the grid. The loading profiles are shown in Table 5.1.

Table 5.1: ZIP parameters of Nordic TSOs [69].

ZIP parameters	Z_p	I_p	P_p	Z_q	I_q	P_q
Constant admittance load model	1	0	0	1	0	0
TSO 1	0.40	0	0.60	0.90	0	0.10
TSO 2	0.25	0.40	0.35	0.70	0.30	0
TSO 3	0.40	0.40	0.20	0.40	0.40	0.20

5.2 Scenario 1: More Wind and Solar Penetration in Southern and Central part of Sweden

According to Network Development Plan 2016-2025 [8], the northern part of Sweden has a high potential for harnessing wind power and attracting attention to economic viability due to its lower population density. The development plan also stated that the southern part of Sweden, particularly the sea area, has a more significant potential for capturing large amounts of wind power. In the Swedish grid, most of the power comes from hydro-power plants situated in the North. As a result, if power capacity increases by constructing more wind farms in Northern Sweden, grid capacity must be reinforced; otherwise, transmission losses would increase, because power is transported over a long distance to the load location (Southern Sweden). Therefore, to reduce the transmission losses, it is better to construct new wind farms close to coastal sites in Southern and Central part of Sweden from the socio-economic point of view [8]. It will reduce network reinforcement to some extent. Since plans on solar PV has not been stated clearly in the development plan, hence the solar PV plants have been placed according to Global Solar Atlas. As published by World Bank Group and documented by Solargis [70], the solar radiation map shows that Southern Sweden has lots of Photo-Voltaic power potential in terms of kilowatt hour per kilowatt peak (kWh/kWp). Hence, solar PV are therefore, located mostly in Southern and Central part.

The renewable power (power from wind turbine and solar PV in megawatt) in different locations in the modified Nordic-32 grid with different penetration levels during simulation (in percentage of total power generation in modified Nordic-32 test grid) is tabulated in Table 5.2 .

Table 5.2: Scenario 1: Wind and Solar PV penetration in different location of Nordic-32 Test Grid:

Wind/Solar	Share Power $[MW]$	Wind Penetration $[MW]$			Solar Penetration $[MW]$		
Penetration	Total (both)	North	South	Central	North	South	Central
0%	0	0	0	0	0	0	0
10%	1150	0	0	230	0	345	575
20%	2669	0	0	460	0	690	1519
30%	3452	0	285	405	56	1035	1671

5.3 Scenario 2: More Wind Penetration in Northern part of Sweden and Solar Penetration in the Southern and Central regions

According to System Development Plan 2018-2027 and Nordic Development Plan (June, 2019) [7], [9] most of the share of new wind turbine installation projects will be located in Northern part of Sweden and North of the Nordic regions by the year 2040, irrespective of the lower local electricity demand. Therefore, the main motivation of placing wind turbines in Northern part of Sweden was driven by two main reasons stated in both the development plans. One of the reason was better wind conditions and the other being easier to get installation permits in less populated areas. Still, wind capacity expansion in Northern part of Sweden would also impact the national grid as a result of changes in the power flow dynamics and higher transmission losses when compared to Scenario 1 due to increased North to South power transportation.

However, since plans on solar PV has not been stated clearly in the development plans stated in this section, the solar PV installations has been distributed mostly in Southern and Central part of Sweden following the same method and justification as in Scenario 1.

The renewable power (power from wind turbine and solar PV in megawatt) in different locations in the modified Nordic-32 grid with different penetration levels during simulation (in percentage of total power generation in modified Nordic-32 test grid) is tabulated in Table 5.3.

Table 5.3: Scenario 2: Wind and Solar PV penetration in different location of Nordic-32 Test Grid:

Wind/Solar	Share Power $[MW]$	Wind Penetration $[MW]$			Solar Penetration $[MW]$		
Penetration	Total (both)	North	South	Central	North	South	Central
0%	0	0	0	0	0	0	0
10%	1150	184	0	46	0	345	575
20%	2669	368	0	92	56	1035	1118
30%	3452	378	100	212	0	1185	1577

6

Case Studies: Results and Discussions

6.1 Impact on Frequency Nadir

The dynamic simulation studies conducted on Scenario 1 and Scenario 2 showed similar trends when it came to frequency response to the N-1 contingency criteria disturbance. Figure 6.1 shows the dynamic simulation conducted on Scenario 1 and Scenario 2 using hydro turbine governors for frequency regulation in the modified Nordic-32 test system with constant admittance load model.

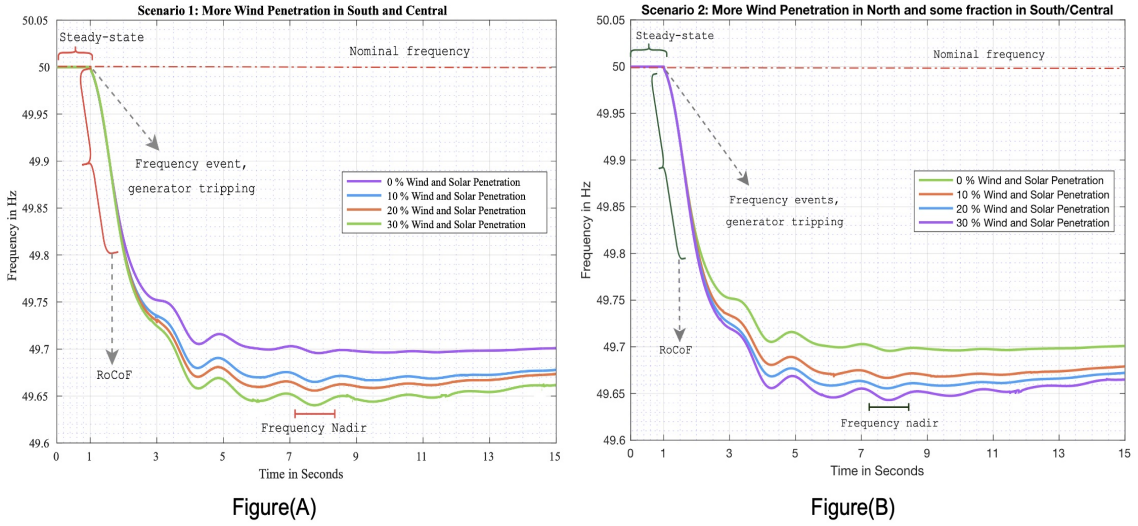

Figure 6.1: Frequency response to N-1 contingency disturbance with frequency regulation from Hydro Turbines in a Constant Admittance load model system; Figure(A) : Frequency response in Scenario 1, Figure(B): Frequency response in Scenario 2.

As can be seen from the Figure 6.1(A), the frequency nadir increases with increase in renewable energy penetration in Scenario 1. Also, oscillations in the frequency response was observed because of the oscillations in the power delivery of the hydro turbines causing it. The final frequency of the system after 15 seconds were also different at different renewable energy penetrations. The frequency responses with different load models also showed similar trend. When the dynamic simulation was conducted on Scenario 2, a similar trend was also observed as shown in Figure 6.1(B).

The behaviors observed confirm our theoretical knowledge and understanding of increase in frequency nadir with increase in renewable energy penetration. The frequency regulation support was changed from the hydro turbines to the ESS and the same dynamic simulation was conducted. The frequency response of the system has been illustrated in Figure 6.2.

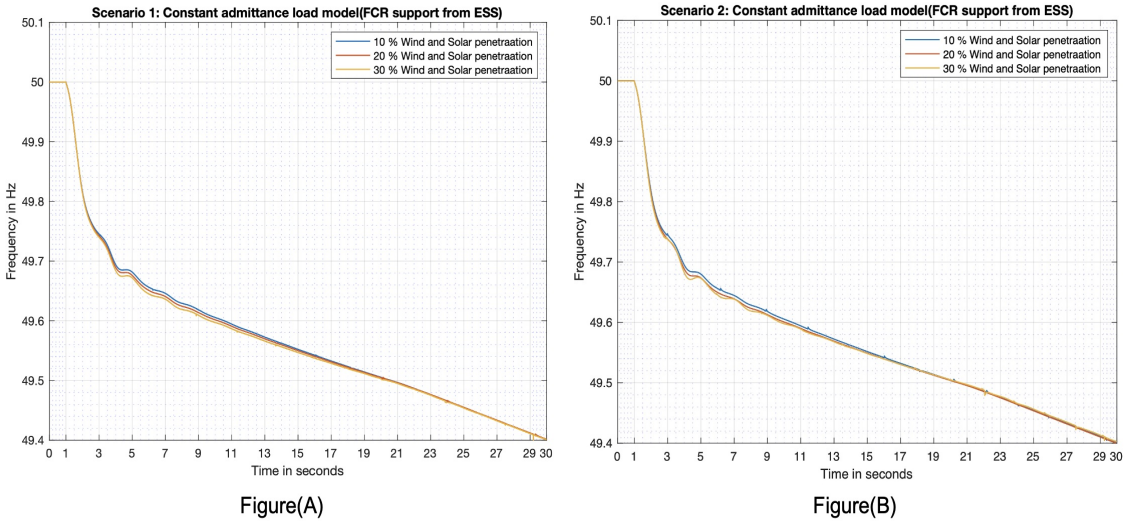

Figure 6.2: Frequency response to N-1 contingency disturbance with frequency regulation from ESS in a Constant Admittance load model system; Figure(A) : Frequency response in Scenario 1, Figure(B): Frequency response in Scenario 2.

As can be seen in Figure 6.2 (A), the initial frequency dip of the system was much smaller compared to that when using hydro turbines for frequency regulation. The initial frequency dip slightly increased with increase in renewable energy penetration and since stated previously that the FCR-D support only would not be sufficient enough to stabilize the frequency, the slow fall of frequency was observed as well. As our case study using ESS relied on achieving the same final frequency at 30 seconds with different renewable energy penetration cases, the final frequency, as can be seen, was the same for all the cases. As for Figure 6.2 (B), Scenario 2 also showed the same trend and behavior as in the case for Scenario 1.

6.2 Impact on FCR-D power and energy requirement

The ESS used for FCR-D support in modified Nordic-32 test system's two scenarios with different load models and renewable energy penetration levels required different amounts of power and energy in order to support the system to have the final system frequency of 49.4 Hz at 30 seconds of dynamic simulation after an N-1 contingency criteria disturbance. For Scenario 1, a comparison between the amount of energy provided by the hydro governor and the ESS for different renewable energy penetration scenarios considering constant admittance load model was provided in Figure 6.3(A), a comparison considering TSO 1 Load Proportion Model was provided

in Figure 6.3(B), with TSO 2 Load Proportion Model in Figure 6.3(C) and TSO 3 Load Proportion Model in Figure 6.3(D). Finally, the maximum power provided by the ESS for different renewable energy penetration scenarios and load proportion models are shown in Figure 6.4.

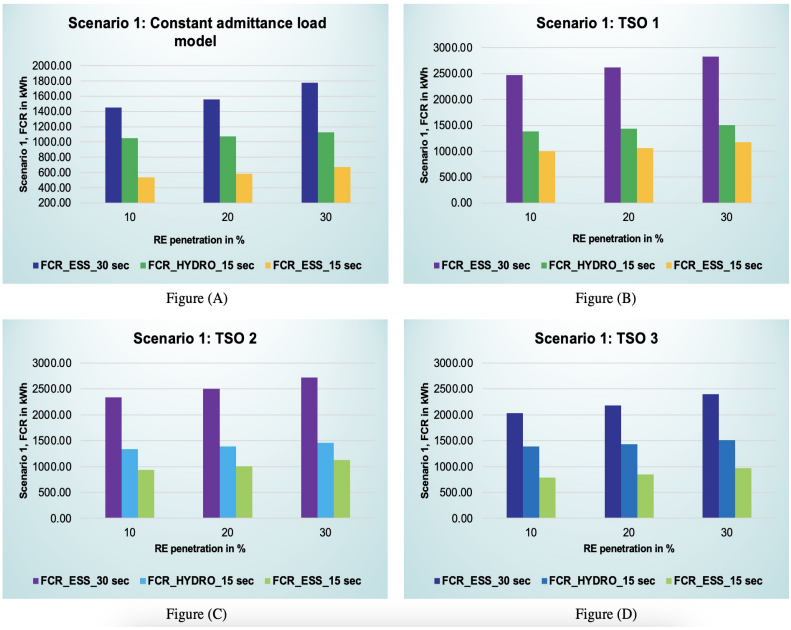

Figure 6.3: Scenario 1 - Variation of FCR-D energy support at different renewable energy penetration; Figure(A): Grid with constant admittance load model, Figure(B): Grid with TSO 1 load proportion model, Figure(C): Grid with TSO 2 load proportion model, Figure(D): Grid with TSO 3 load proportion model.

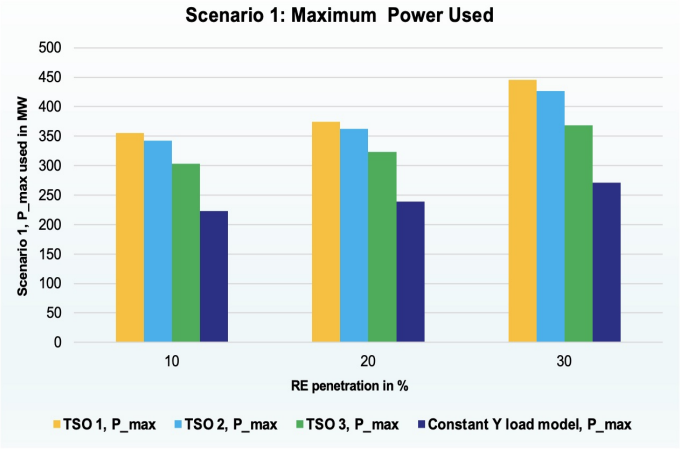

Figure 6.4: Scenario 1 - Maximum power used by ESS at different renewable energy penetrations and load proportion models.

As can be seen from Figure 6.3, the amount of energy provided by the ESS was lower than hydro turbines in the first 15 seconds, which is indicative that the power provided from ESS was not sufficient enough to stabilize the frequency and so the

frequency keeps falling down at a slow rate. The energy requirement was seen to increase with higher renewable energy penetration with the highest amount of energy requirement seen for TSO 1 load model. As for Figure 6.4, the results show that the maximum power from the ESS increased with increase in renewable energy penetration in order to keep the system frequency to 49.4 Hz at 30 seconds of dynamic simulation. The TSO 1 load model required the highest power among the other load models to do so.
The behavior of the power and energy requirement seen in the case of Scenario 1 was also similar in Scenario 2 as Figure 6.5 and Figure 6.6 indicates.

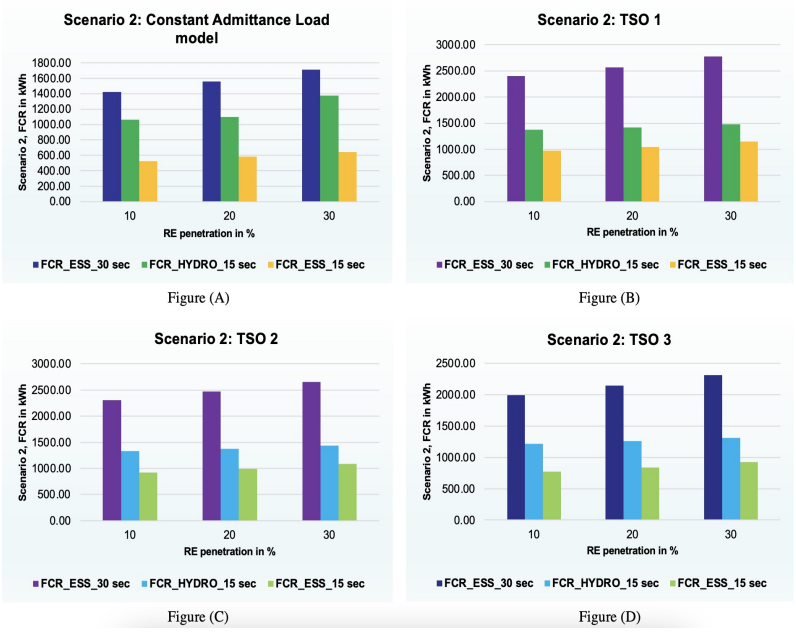

Figure 6.5: Scenario 2 - Variation of FCR-D energy support at different renewable energy penetration; Figure(A): Grid with constant admittance load model, Figure(B): Grid with TSO 1 load proportion model, Figure(C): Grid with TSO 2 load proportion model, Figure(D): Grid with TSO 3 load proportion model.

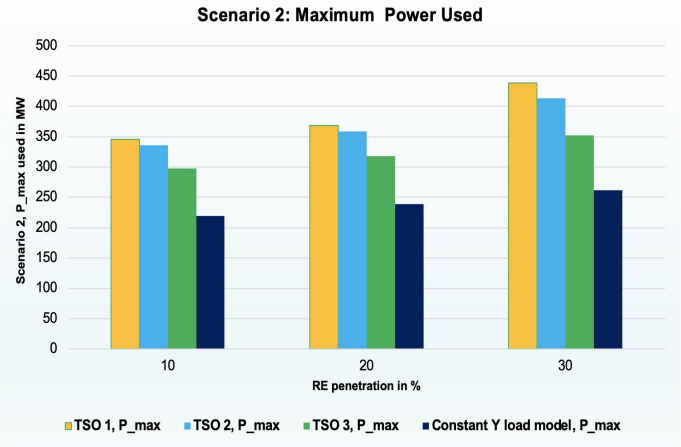

Figure 6.6: Scenario 2 - Maximum power used by ESS at different renewable energy penetrations and load proportion models.

However, after comparing, it was seen that the power and energy requirement from Scenario 1 was slightly higher than Scenario 2. The results from Scenario 1 and 2 showed that the maximum power requirement for both the scenarios had a slight difference of around 2% on average with Scenario 1 having the higher power requirement. In theory, since the location of power delivery for FCR-D support remains constant for both cases, the power requirement for the same disturbance should be the same. However, this change can occur since these are two different scenarios with different bus voltage variations and power flows through the transmission lines during the dynamic simulation which can constitute to such small change in the power requirement.

As stated previously, the results indicated that the power and energy provided by the ESS increased with increase in renewable energy penetration among both Scenario 1 and Scenario 2 and similar trend was also observed with different load profile models with highest power and energy supplied with the load profile model of TSO 1 and minimum with Constant Admittance Load profile model. To explain the reason behind the phenomena, some other related factors were necessary to be investigated.

There are three types of load categories which can be used in PSS®E; Constant Power, Constant Current and Constant Admittance load models. When the loads are converted, the program uses the initial bus voltage of the load and calculates the current and admittance of the load. By doing so, the value of power, current and admittance is kept constant, depending upon the type used, during the dynamic simulation. When the N-1 contingency disturbance occurs, we noticed that the bus voltages of the load busses drop which can be seen in Figure 6.7.

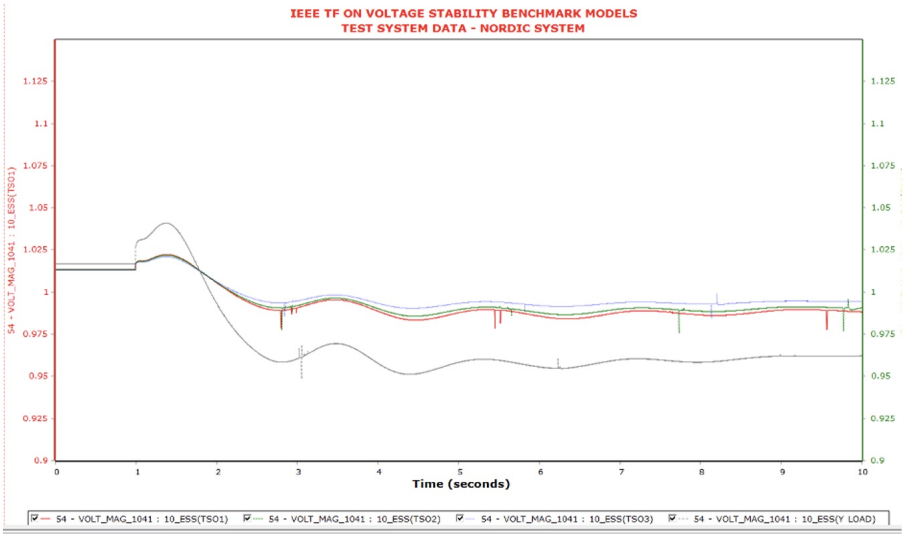

Figure 6.7: Load bus voltage with different load models after N-1 contingency disturbance.

The load proportions used as cases for different scenarios can be seen in Table 5.1 showing the various proportions of different load models. From the figure 6.7, We notice that the voltage drops to a lower value and the values are quite similar for TSO 1, TSO 2 and TSO 3 but for constant admittance load model the voltage drops further. For this reason, the total power consumption from the constant admittance load model drops significantly and so the power requirement from the FCR support is significantly lower compared to the other load models. As for the other load models, since the voltage drop is quite similar for these cases, that means the power consumption for the constant current and the constant admittance load drops. However, since TSO 1 has a higher constant power load, so the total load does not drop as much compared to the other load models. Hence, more FCR power was required to balance the load for TSO 1 load model and less for Constant Admittance Load model.

6.3 Impact on Performance of FCR-D support

In the previous studies with different scenarios, it came to light that with the use of ESS, the initial frequency dip was much smaller compared to that of using hydro turbines. However, the power delivery from the ESS has been modelled taking into consideration the technical specification guidelines specified in [21] and as depicted in the stationary performance requirements, the ESS should activate from 49.9 Hz with maximum activation at and below 49.5 Hz. On the other hand, the hydro turbines in the Nordic-32 test system, has droop settings of the hydro governors set to 4% for G1-G5, G8-G12 and 8% for G19-G20 respectively. So more detailed study needs to be carried out to understand the performance of the ESS and how it impacts the performance of FCR-D support.

For this reason, a dynamic simulation study was carried out in Scenario-1 with 10% renewable energy penetration where the simulation was run at steady state for 1 seconds before a loss of generation in the form of tripping generator G10 was simulated and later the simulation was run for 30 seconds. The system frequency behavior with hydro turbines for frequency regulation was first observed and later the frequency regulation from ESS was activated and the maximum power of the ESS was varied such that the final frequency of the system at 30 seconds becomes similar in both cases and that the power delivered by both the sources at that time are close to each other. Figure 6.8 illustrates the results obtained in the simulation.

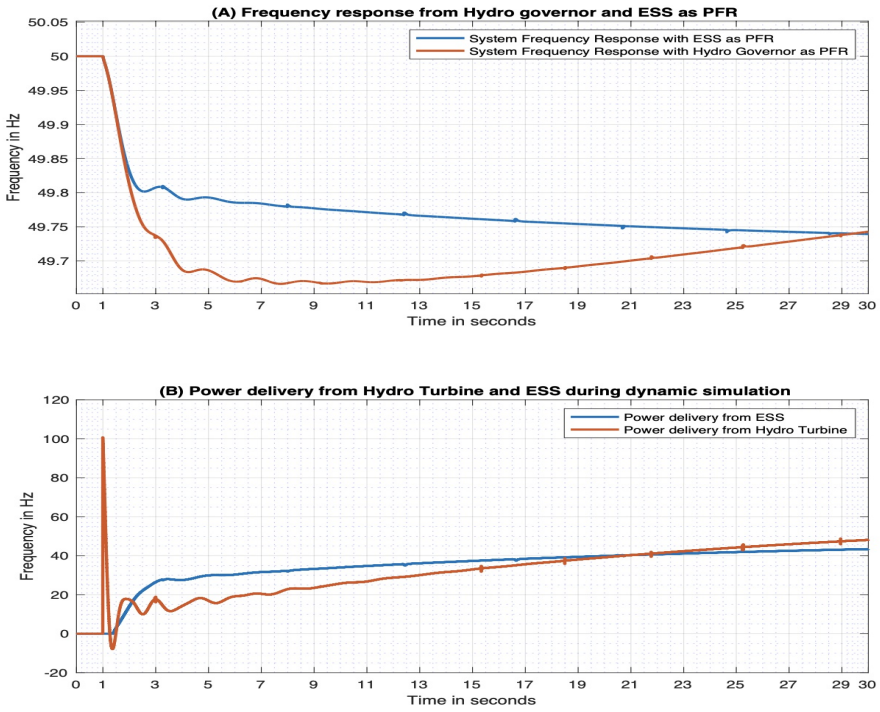

Figure 6.8: Performance evaluation of Hydro Governor and ESS. (A) System Frequency Response with N-1 contingency disturbance with Hydro Governor and ESS as PFR. (B) Power Delivery from Hydro Turbine and ESS during Dynamic Simulation.

As can be seen from the figure, the power delivered from the ESS was much faster compared to the hydro turbine which resulted in smaller dip in frequency compared to that with hydro governor as the frequency regulator. Even though the droop constant of the hydro governor was small, it was still not able to ramp up its power as fast as the ESS. This is due to the oscillations in the governor mechanical system, where the transfer function of the servomotor of the governor, controlling the mechanical torque to the turbine, has various time constants for the controller which causes such behavior. From the simulation, it was confirmed that the ramp up rate for the hydro turbine after the inertial response (from 1.855 to 2.515 seconds) was 12.0 MW/s whereas during the same time, the ramp up rate for the ESS was around 17.216 MW/s. In order to observe the change in behavior with higher renewable energy penetration and different dynamic load, Scenario 2 with 30% renewable energy penetration and

TSO 1 as the load model was used as the case study. The dynamic simulation study showed that the ramp up rate for the hydro turbine after the inertial response was also close to 12 MW/s since we did not change its characteristics whereas after changing the maximum power of the ESS to reach the same system frequency at 30 seconds as that in the case with hydro turbines, the ramp up rate for the ESS was able to increase to 25.89 MW/s. This was possible because since the ESS has a very fast power delivery which depends upon the trajectory of frequency change and the maximum power delivery value, the ESS can ramp up its rate according to the rate of change of frequency, whereas in case for the hydro turbine, the ramp up rate remained similar in both cases indicating that the controller for the servomotor being the bottleneck for its power delivery, was not able to provide better frequency regulation support at higher renewable energy penetrated grid systems. The results showed ESS as being a better candidate for FCR-D support in terms of performance of power delivery as well as adaptability with changes in renewable energy penetration in the system.

6.4 Impact on Overall Cost of FCR-D support

To investigate the impact ESS makes on overall cost of FCR-D support, we first need to calculate the overall cost of FCR-D with the use of traditional sources which we will take as our base case. In Chapter 2, we have seen that the price of FCR-D is bid in the balancing market. The price of FCR-D vary significantly, however there is an underlying trend to the pricing. According to [5], most of the FCR-D support in Sweden is provided by hydro turbines and so the operators charge more for per unit if the amount of power to be reserved for FCR-D is high. The reason for it is that, in case of FCR-D downward support, large power support from the hydro turbines would make the turbines to operate at a lower capacity which in turn decreases the efficiency of the plant as well as the revenue the plant makes. So to compensate for the loss, the operators charge a higher premium for the FCR-D support. In case of FCR-D upward support, the hydro turbines are needed to run at a higher power capacity which reduces the reservoir level from their reference base line and so in the long run the water level would not be high enough for power production, also reducing their revenue. So to compensate for the loss in revenue due to lower power production in the long run, the price of FCR-D upward increases with high power support requirement.

The prices of FCR-D support from the last three years have been extracted from Fingrid open source platform [74] and illustrated in Figure 6.9.

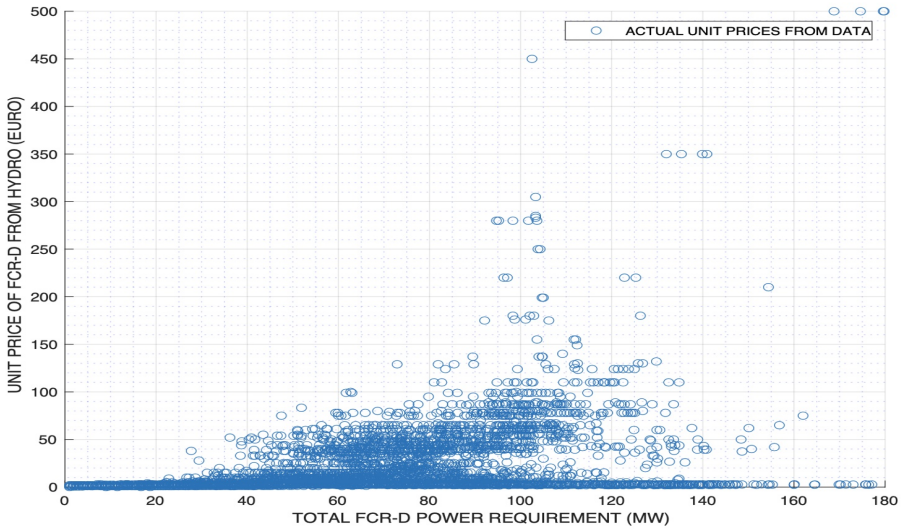

Figure 6.9: Scatter plot with data of unit prices (EURO) of FCR-D from 2017-20.

As can been seen, the actual prices do not provide any clear mathematical relation with the amount of FCR-D power requirement. However, the data was conditioned to provide average prices for a range of power requirements and doing so a mathematical best fit representation of the price can be achieved. Figure 6.10 shows the best fit line that was estimated to be the unit prices of FCR-D support from traditional energy sources.

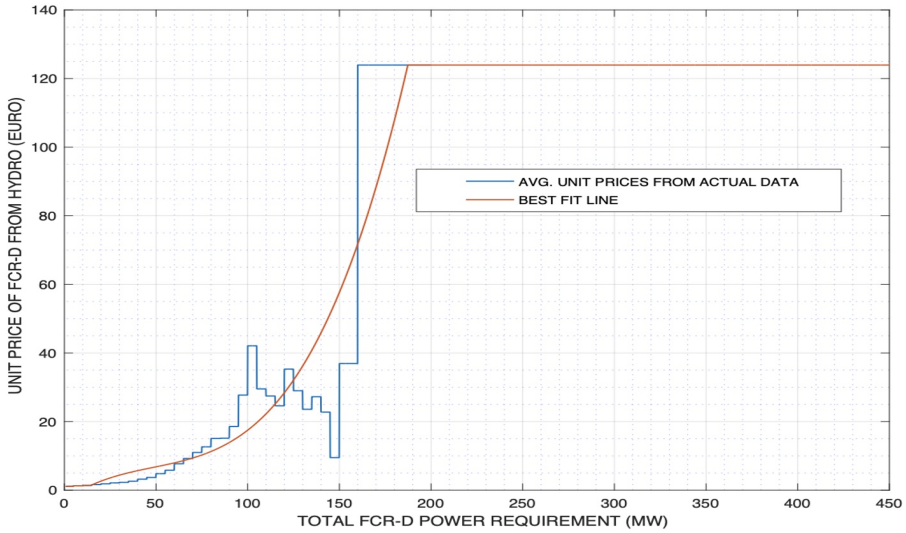

Figure 6.10: Average unit prices (EURO) of FCR-D from Hydro Turbines including a mathematical fitting function.

As seen, the unit prices of the FCR-D from traditional sources increases with increase in power requirement at an exponential rate and reaches a maximum value at around

187 MW. This unit price was kept constant with further increase in power requirement since it was assumed to be the maximum price of FCR-D from traditional sources. By using the unit prices of FCR-D from traditional sources, the overall cost of FCR-D at different power requirement levels can be calculated. Figure 6.11 provides the overall cost of FCR-D support at different power requirement levels.

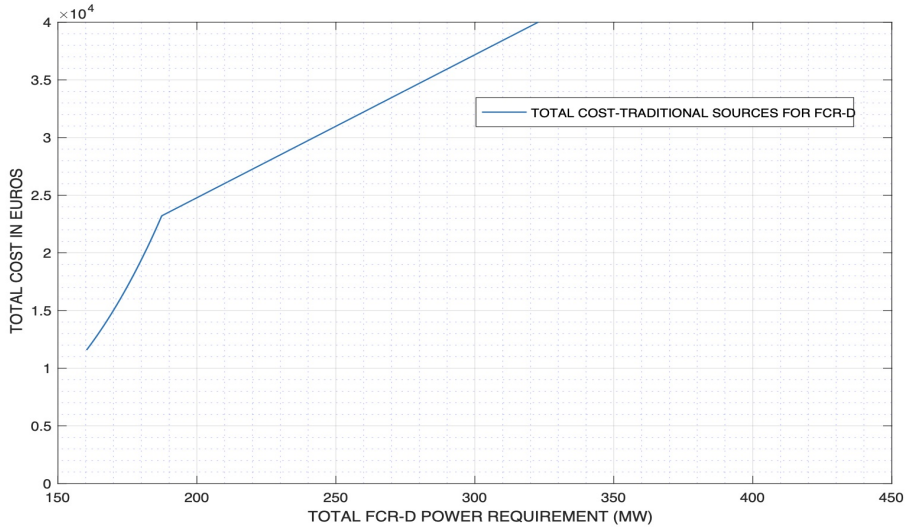

Figure 6.11: Average unit prices (EURO) of FCR-D from Hydro Turbines including a mathematical fitting function.

As can be seen from the Figure, the overall cost of FCR-D increases exponentially with increase in power requirement and then bove a power requirement of 187MW, due to the constant maximum unit price of FCR-D, the overall cost increases linearly. In conclusion,the overall price increases significantly and at exponential rate with increase in FCR-D power requirement.

Since we have now established the base case, we can move into investigating the impact of ESS on overall cost of FCR-D support. In chapter 3, we have looked into the method for calculating the LCC and also the unit prices of ESS. By using the methods, we calculated the unit prices of ESS using different energy storage sources using the prices for the year 2020 and also the estimated prices of the year 2030 and the results obtained from the calculations has been illustrated in Figure 6.12 together with the unit price of FCR-D from traditional sources for a comparative viewpoint.

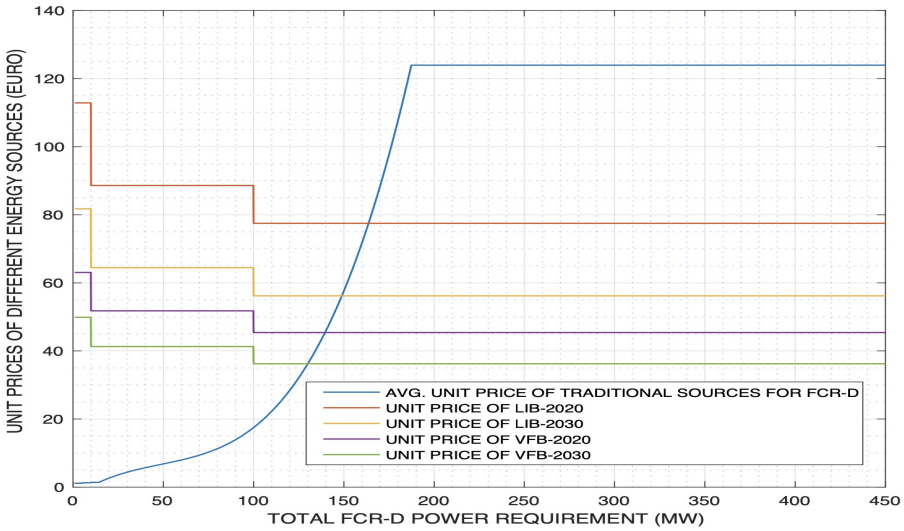

Figure 6.12: Unit price (EURO) of FCR-D provided by traditional sources for FCR-D, Lithium-ion and Vanadium Redox Flow Battery based ESS.

As can be seen from the figure, the unit price of FCR-D support from traditional sources is very economical when the total FCR-D power requirement is low but with higher power requirements, the price increases exponentially making the price of Lithium-ion battery and Vanadium redox flow battery based ESS much more attractive.

In the near future, the dependence upon frequency containment reserves such as FCR-D would be much higher due to the imminent renewable energy penetration in the electrical grid. As seen from Figure 6.11, with higher requirement of FCR-D support, the total cost would increase exponentially which would ultimately impact on the price of electricity. However, since the prices of FCR-D support from ESS reduces as the power requirement becomes higher as seen in Figure 6.12, the use of FCR-D support from ESS as a compliment to the FCR-D support from traditional energy sources could provide substantial reduction in the overall cost. A numerical method which calculates the estimated overall cost of FCR-D support using the combination was developed in **MATLAB** software which provides the proportion of power from ESS and from traditional sources for FCR-D support to obtain the lowest possible overall cost of FCR-D support. The numerical solver goes through all the possible combinations of power delivery (with 1MW increments) and extracts the one with the lowest overall cost.

The method was used for ESS with Lithium-ion battery and Vanadium redox flow battery based ESS separately as the source with prices from the year 2020 and also the estimated prices for the year 2030. Figure 6.13 shows the percentage of total power requirement for FCR-D to be provided by ESS with Lithium-ion Battery as the source to achieve the minimum overall cost of FCR-D support. As can be seen, the percentage of power from ESS is higher than traditional FCR-D sources when the FCR-D power requirement exceeds 180 MW for the prices from the year 2020 and 170 MW for the prices from the year 2030. Figure 6.14 shows the percentage of

total power requirement for FCR-D to be provided by ESS with VRFB as the energy source to achieve the minimum overall cost of FCR-D support. As can be seen, the percentage of power from ESS was higher than traditional FCR-D sources when the FCR-D power requirement exceeds 165 MW for the prices from the year 2020 and lower than 160 MW for the prices from the year 2030. In both cases, the percentage of power from ESS showed an increasing trend with higher overall FCR-D power requirement.

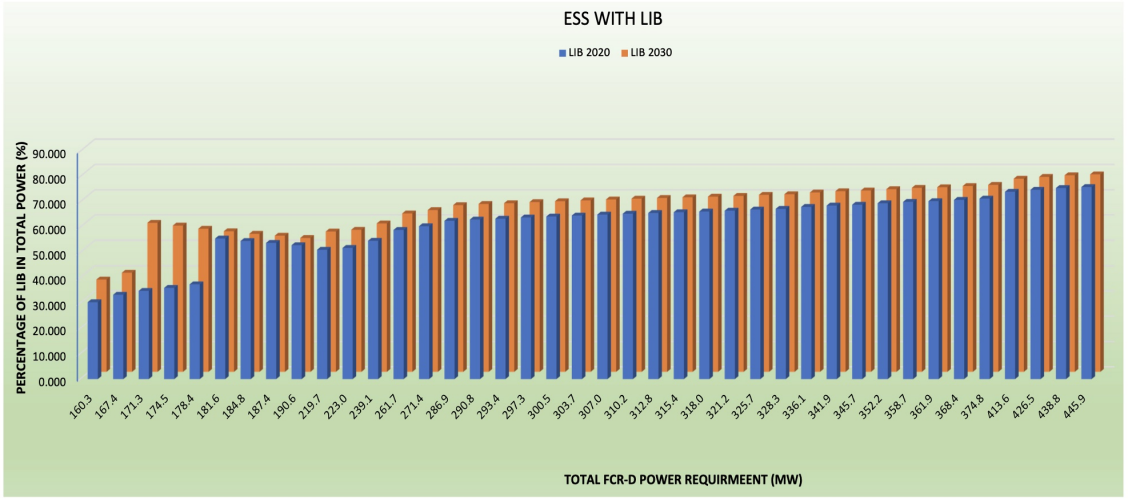

Figure 6.13: Percentage of Lithium-ion battery based ESS in the total FCR-D power requirement.

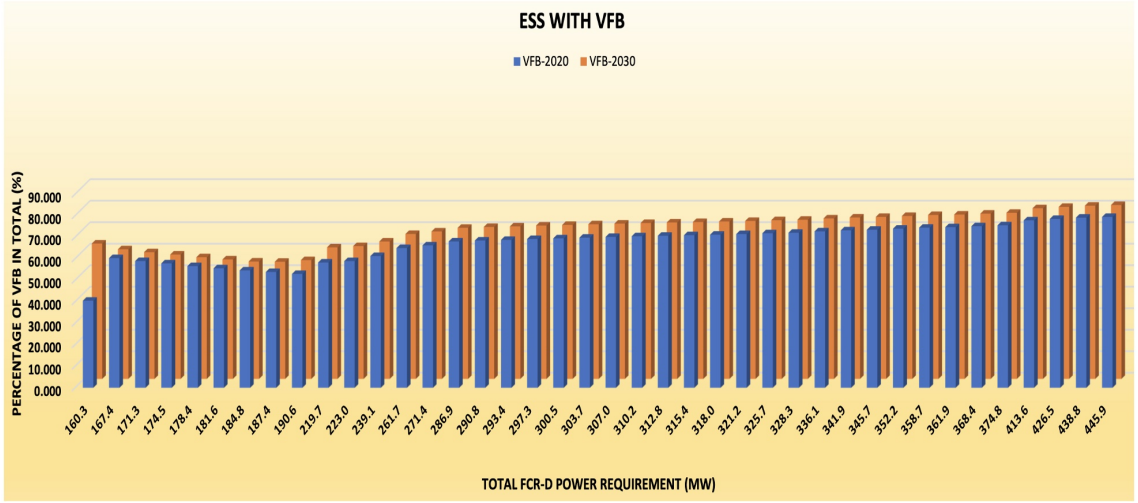

Figure 6.14: Percentage of Vanadium Redox Flow battery based ESS in the total FCR-D power requirement.

Finally, the total overall cost of FCR-D support with different energy storage source combinations has been shown in Figure 6.15. The results show that the overall cost of FCR-D support with traditional FCR-D energy sources and Lithium-ion battery based ESS combined was found to be a minimum of 40% lower than the overall cost of

FCR-D support from traditional FCR-D sources only, with total FCR-D requirement of 160 MW and above. If the price of Lithium-ion battery for the year 2030 were used, then the overall cost of FCR-D support can be reduced by a minimum of 51.2%. Also, the overall price of FCR-D support can be reduced by a minimum of 57.2% and 63.5% using VRFB as the source of ESS with prices from year 2020 and 2030 respectively. However, according to the unit prices, the FCR-D support from ESS is only economical when the total FCR-D power requirement is 140MW from the year 2020 and 131 MW from the year 2030.

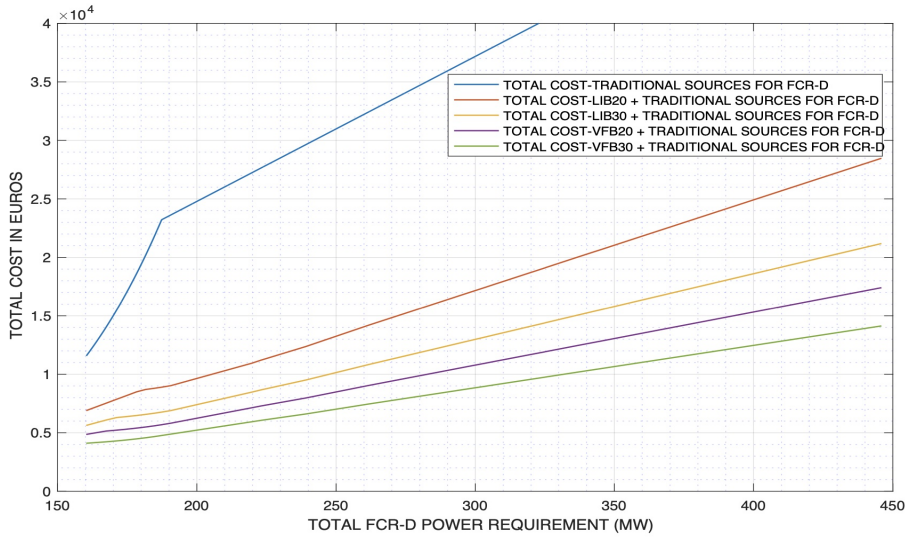

Figure 6.15: Total cost (EURO) with FCR-D support different combinations of energy sources.

6.5 Discussions on system behavior during dynamic simulations

The main objective of the thesis was to observe the frequency response of a modified Nordic-32 grid with renewable energy penetration. The task of modifying the Nordic-32 test system by itself was very laborious. The test system had to be balanced after each modification such that the transmission lines in the test system were not overloaded and the bus voltages needed to be within a reasonable range, requiring hours on changes and trial and error process. From our studies, many findings have been predictable and satisfied our literature review while others have not been what we expected.

6.5.1 Oscillations in the frequency response to N-1 contingency disturbance

The dynamic simulations consisting of hydro turbines as being the primary frequency regulator resulted in frequency responses with small but significant low frequency oscillations. Figure 6.1 (A) illustrates this behavior in case of Scenario 1 which was

also similar for Scenario 2. This oscillation in the frequency can be explained by the response of the power generation from the Hydro Turbines after the disturbance occurs. Figure 6.16 illustrates the frequency and power responses from two cases where the primary frequency regulation was provided by the hydro governors in Figure 6.16(A) and provided by ESS in Figure 6.16(B). This figure can be used as a tool to explain the reasoning. As can be seen, due to the dynamic model and behavior of the hydro turbine generator G20, just like any other hydro turbines present in the test system, increases their power output having oscillations while doing so. This is due to the dynamic data such as Water Time constant and Gate time constant and also the response from the PI controller, causing the servomotor model of the turbine to provide oscillations in its output. Thus as the power oscillates, it impacts the frequency causing oscillations. This behavior is absent in Figure 6.16(B) because since the power output response of ESS is linear droop control, the power output from it is only dependent upon the frequency and so there is no oscillation. A small oscillation at the beginning of the frequency dip is only present due to the inertial response from the rotating machines in the test system.

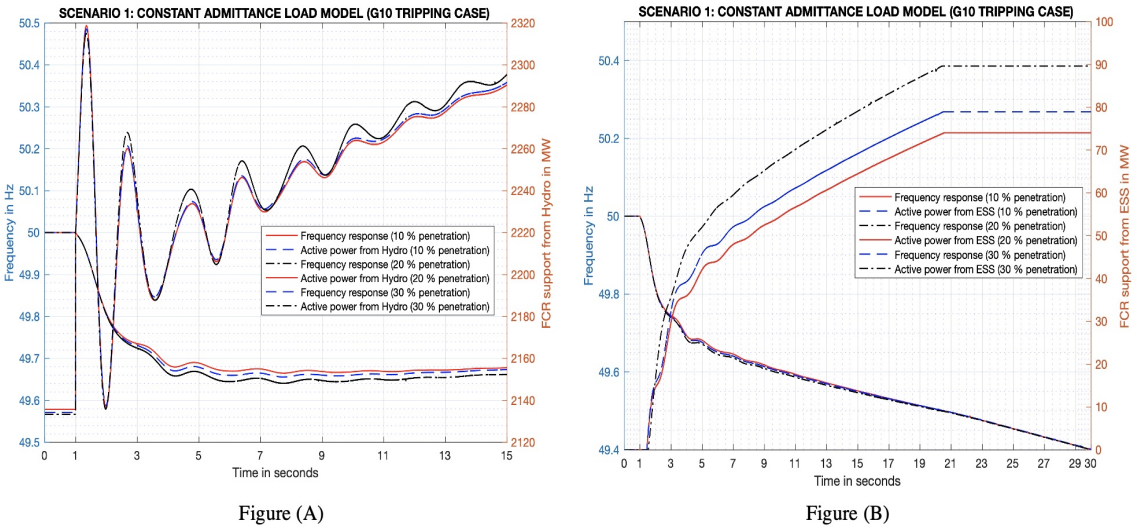

Figure 6.16: Frequency Response to N-1 Disturbance with Constant Admittance load model grid with Hydro Governor and ESS activated for Frequency Response.

6.5.2 Abrupt changes in the frequency responses during Dynamic Simulations

In many of our dynamic simulations with Scenario 1 and Scenario 2, abrupt changes in the data during dynamic simulations were observed where the frequency plot would show very fast changes in frequency which were unlike to the actual trend of the response. Figure 6.17 showed the same behavior. The results obtained were based upon tweaks to the dynamic simulation solution parameters which were able to minimize these abrupt changes but were unable to eliminate them. Upon further investigation, it was found that the problem was in the software side. The PSS®E 35.0 software was facing problems while providing numerical solutions during the

dynamic simulation with cases containing wind turbine and solar PV models. At some instances during the dynamic simulations, the network did not converge even though the initial conditions were checked to be O.K. before the dynamic simulations were started. This could only mean that the software suffered a failure in the numerical solution during the simulation which could not be solved by us. However, the dynamic simulation works completely fine when there were no wind turbine or solar PV models in the network which can be seen from the dynamic simulation results with a theoretical study with reduced system kinetic energy which can be seen in Figure 6.18.

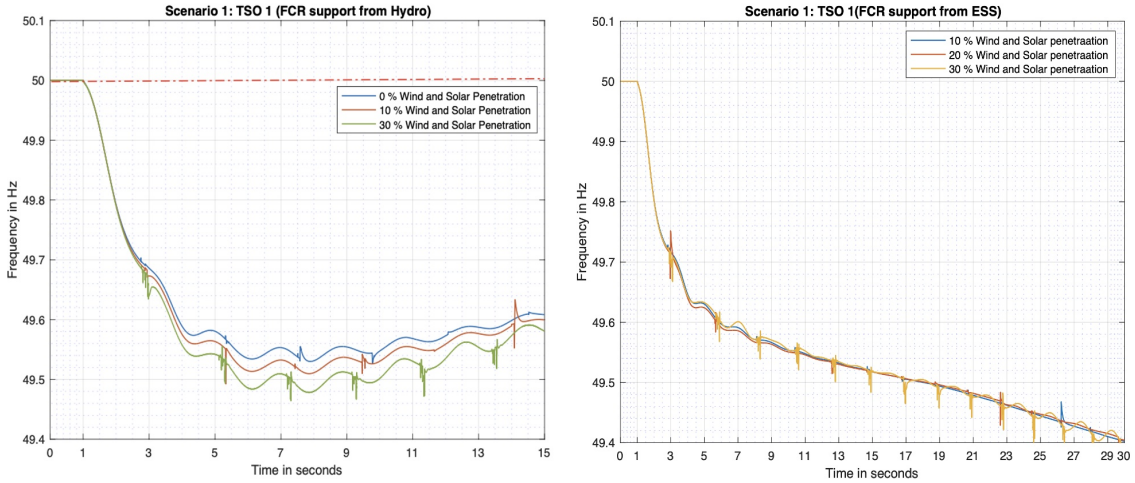

Figure 6.17: Frequency response to N-1 contingency disturbance with TSO 1 load proportion model; Figure(A) : Frequency regulation through Hydro governors, Figure(B): Frequency regulation through ESS.

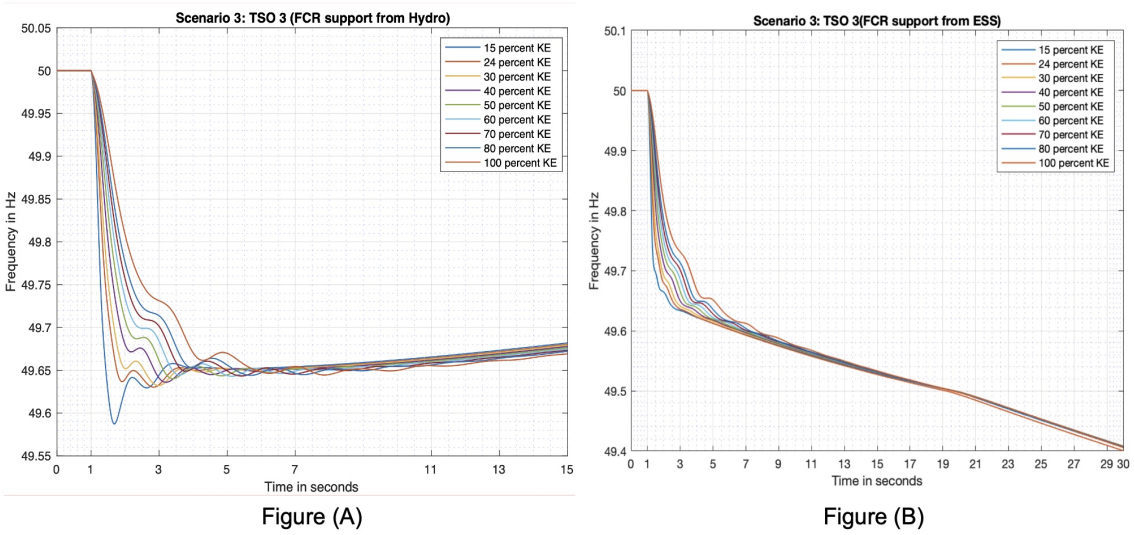

Figure 6.18: Frequency response to N-1 contingency disturbance with TSO 3 load proportion model; Figure(A) : Frequency regulation through Hydro governors, Figure(B): Frequency regulation through ESS.

6.6 Sustainable Aspects

Energy Storage Systems (ESS) with Lithium Ion and Vanadium Redox Flow Batteries would be a good solution for fully utilizing renewable sources and reducing plant curtailment. As a result, the United Nations Sustainable Development Goals (UNSDGs) of using clean energy and reducing carbon emissions into the ecosystem would be met [1]. However, there are some negative environmental impacts associated with large-scale lithium production and Lithium-Ion battery end-of-life processing [73], [79]. The salt lakes in Chile account for 40% of the world's lithium reserves and the extraction process of lithium may lead to irreversible impacts on the local valuable ecosystems [79]. Thus, proper management strategies and policies facilitating recovery, recycling, and reuse of waste lithium ion batteries s at different levels are needed.

6.7 Ethical Aspects

The future electrical grid will incorporate a significant amount of renewable energy. The lower generation cost of renewable energy sources has substantial benefits making it the ideal choice. However, as previously discussed, large-scale implementation would weaken and destabilize the grid. The proposed solution addresses such issues, allowing for the smooth and proper performance of large-scale renewable energy plants while minimizing renewable energy curtailment without making the electrical system vulnerable and weak. As a result, the goal of affordable electricity would be realized. Countries' development would accelerate; poverty-stricken countries would be able to provide necessary facilities to their people due to lower electricity costs such as clean water. The benefits to humanity are limitless, and this thesis work provides a glimpse into a greener world.

7

Conclusion and Future Work

7.1 Conclusion

The thesis provided a foundation of the economic advantages of using Energy Storage Systems (ESS) in the future when the electrical grid will be heavily dependent upon frequency regulation services due to the increase in renewable energy penetration. The study was conducted on a modified Nordic-32 test system with various percentage of renewable energy penetration from wind turbines and solar PVs.

With regards to our first objective of the thesis, the results found from different scenarios and case studies provided a clear picture of the increased dependence in FCR-D service with higher renewable energy penetration in the modified Nordic-32 test system. With regards to our second objective of the thesis, the case studies showed that the power delivery from the ESS was quite fast and flexible compared to the power delivery from hydro turbines. The results also indicated that with higher renewable energy penetration, the ESS was able to increase the ramp up rate of power delivery from 17.216 to 25.89 MW/s which resulted in much smaller frequency nadir compared to that of hydro turbines whose ramp up rate remained almost constant at 12.0 MW/s through different scenarios. Finally with regards to our third and final objective, studies have found that using ESS as a compliment with the traditional sources for FCR-D services for overall power requirement higher than a certain value, the combination provided significant economical benefits on the total cost of FCR-D services. The overall cost of FCR-D services can be reduced by a minimum of 40% when the overall FCR-D requirement is higher than a certain power level for the year 2020 and by 51% for the year 2030.

The challenges for implementing large amount of renewable energy sources for power generation into the electrical grid are huge but solutions are there to make it happen. The use of ESS can provide both stability and economical benefits for the grid and would be able to reduce the cost of electricity which was our main aim all along.

7.2 Limitations and Future Works:

When it comes to limitations, our thesis study provided a rather simpler interpretation of the unit price of the Lithium-ion and Vanadium Redox Flow Battery based ESS using Life Cycle Cost Assessment. Even though it provides a foundation, however it cannot determine the exact price of them. This statement is also true

for the unit price of FCR-D supplied from traditional sources. We got the data for FCR-D support from traditional sources and made a lot of assumptions and conditioning to estimate the unit prices. However, in the present time it is much more complicated as there are other factors determining the prices of FCR-D in the balancing market and our simplified model may contain large amount of inaccuracy since the price is always bid in the balancing market which have high variance and may increase or decrease over time.

The thesis was based on a specific topic which has numerous branches that can be researched upon. So, future work can be done by using a better model for pricing of the FCR-D support from traditional FCR-D sources and from ESS for more practical results. Also, optimization and sensitivity analysis of the ESS's technical performance, as well as the pricing of traditional FCR-D sources and the ESS, can be carried out for more realistic and accurate results. Finally, work on finding the optimum locations of the FCR-D support as well as finding the method to provide optimum delivery of power from the ESS using machine learning can also be looked at.

Bibliography

[1] Ensure access to affordable, reliable, sustainable and modern energy. [Online]. Available: https://www.un.org/sustainabledevelopment/energy/

[2] IEA, Installed power generation capacity in the Stated Policies Scenario, 2000-2040, IEA, Paris https://www.iea.org/data-and-statistics/charts/installed-power-generation-capacity-in-the-stated-policies-scenario-2000-2040.

[3] "Why does the cost of renewable energy continue to get cheaper?," 2019

[4] "IEA Wind Task 26: The Past and Future Cost of Wind Energy," 2012.

[5] Hjalmar Pihl, November 2019. Swedish FCR prices – an analysis of the data. Available from: https://www.ri.se/sites/default/files/2021-02/Swedish-FCR-prices_1.pdf

[6] Ørum et.al. Future System Inertia 2. A report by the Nordic TSOs. Available at: https://www.statnett.no/globalassets/for-aktorer-i-kraftsystemet/utvikling-av-kraftsystemet/nordisk-frekvensstabilitet/future-system-inertia-phase-2.pdf

[7] System Development Plan 2018–2027, Svenska Kraftnät [online]. Available: https://www.svk.se/siteassets/om-oss/rapporter/2018/svenska-kraftnat-system-development-plan-2018-2027.pdf

[8] Network Development Plan 2016 – 2025, Svenska Kraftnät. [online]. Available: https://www.svk.se/contentassets/c7ff3f2bb5ed4d4a8d7d6d0599a5426a/network-development-plan-2016-2025_webb.pdf

[9] Nordic Development Plan , June 2019. [online]. Available: https://via.tt.se/data/attachments/00885/1ffd1736-26c5-4a66-9f0d-09bb8a8efbcf.pdf

[10] P. Kundur et al., Power System Stability and Control. New York, NY, USA: McGraw-Hill Education, 1994.

[11] Thomée, Lucas, 'Lithium-Ion Battery Storage for Frequency Control'. [online]. Available: https://hdl.handle.net/20.500.12380/255343.

[12] Pieter Tielens, Dirk Van Hertem, The relevance of inertia in power systems, Renewable and Sustainable Energy Reviews, Volume 55, 2016, Pages 999-1009, ISSN 1364-0321, https://doi.org/10.1016/j.rser.2015.11.016.

[13] V. Knap et al., (2016). 'Sizing of an Energy Storage System for Grid Inertial Response and Primary Frequency Reserve'. I E E E Transactions on Power Systems, 31(5), 3447-3456. https://doi.org/10.1109/TPWRS.2015.2503565

[14] A. Danell et al., "Nordic Future System Inertia," European Network of Transmission System Operators for Electricity (ENTSO-E), Brussels, Belgium, 2015. [Online]. Available: https://bit.ly/3e0eLil.

[15] Gonzalez-Longatt, Francisco. (2019). Frequency Control in Low Inertia Systems: Non-Synchronous Technologies. Available: https: 10.13140/RG.2.2.36834.27841

[16] M. M. N. Rezkalla et al., (2018). Electric Power System Inertia: Requirements, Challenges and Solutions. Electrical Engineering, 100(4), 2677-2693. https://doi.org/10.1007/s00202-018-0739-z.

[17] L. Meng et al., "Fast Frequency Response From Energy Storage Systems—A Review of Grid Standards, Projects and Technical Issues," in IEEE Transactions on Smart Grid, vol. 11, no. 2, pp. 1566-1581, March 2020, doi: 10.1109/TSG.2019.2940173.

[18] Guidance on the provision of reserves, Svenska Kraftnät. [online]. Available: https://www.svk.se/siteassets/aktorsportalen/elmarknad/information-om-stodtjanster/guidance-on-the-provision-of-reserves.pdf.

[19] Gonzalez-Longatt et al., 2014. Power Factory applications for power system analysis.

[20] D. Karlsson et al., IVA-projektet Vägval el, 2015. "Svängmassans roll i framtida elsystem', Gothenburg, Gothia Power", [Online]. Available: https://www.iva.se/globalassets/rapporter/vagval-el/201606-iva-vagvalel-svangmassa-c.pdf.(Swedish)

[21] Technical Requirements for Frequency Containment Reserve Provision in the Nordic Synchronous Area (17 March 2021). Available : https://www.svk.se/contentassets/20aec45c5ea74f7a9557bf3413d03b16/fcr-technical-requirements.pdf

[22] Ilari Alaperä, 'Flexibility services in the Nordics with Datacenters', Fortum Spring. [online]. Available: https://www.svk.se/contentassets/0ac91b8aacb44cbebc55de98b15d14ee/svk-datacenter-fortum-spring.pdf.

[23] Linda Thell, 'Market design and conditions', Svenska Kraftnät. [online]. Available: https://www.svk.se/contentassets/0ac91b8aacb44cbebc55de98b15d14ee/market-design-and-conditions-final.pdf.

[24] 'System Operation Agreement 2018-06-12', ENTSO-E.

[25] Fast frequency response (FRR), Svenska Kraftnät. [online]. Available: https://www.svk.se/aktorsportalen/systemdrift-elmarknad/information-om-stodtjanster/ffr/

[26] Niklas Modig et al., Technical Requirements for Fast Frequency Reserve Provision in the Nordic Synchronous Area, ENTSO-E. [online]. Available: https://www.svk.se/siteassets/4.aktorsportalen/natverksamhet/tekniska-riktlinjer/ovriga-instruktioner/technical-requirements-for-fast-frequency-reserve-provision-in-the-nordic-synchronous-area-eng.pdf.

[27] AEMC, Fast frequency response market ancillary service, Draft rule determination, 22 April 2021.

[28] Nordic Balancing Philosophy, Svenska Kraftnät. [online]. Available: https://www.svk.se/en/stakeholder-portal/Electricity-market/nordic-balancing-philosophy/

[29] Abolfazl Khodadadi et. al., Nordic Balancing Markets: Overview of Market Rules. [online]. Available: https://www.diva-portal.org/smash/get/diva2:1457879/FULLTEXT01.pdf

[30] A nearly complete list of European TSOs. [Online]. Available: https://www.next-kraftwerke.com/knowledge/european-tsos-list

[31] Nordic grid code 2007 (Nordic collection of rules). [Online]. Available: https://eepublicdownloads.entsoe.eu/clean-documents/pre2015/publications/nordic/planning/070115_entsoe_nordic_NordicGridCode.pdf
[32] P. K. e. al., "Definition and classification of power system stability IEEE/CIGRE joint task force on stability terms and definitions," IEEE Transactions on Power Systems, vol. 19, pp.1387-1401, 2004
[33] 'Slutrapport pilotprojekt Flexibla hushåll', Svenska Kraftnät, [Online]. Available: https://www.svk.se/siteassets/om-oss/rapporter/2017/slutrapport-pilotprojekt-flexibla-hushall.pdf.
[34] Houmøller AP. Scandinavian experience of integrating wind generation in electricity markets. In: Jones LE, editor. Renew. Energy Integr. 2nd ed., Boston: Academic Press; 2017, p. 55–68. 10.1016/B978-0-12-809592-8.00005-6 [chapter 5]
[35] An overview of the Nordic Electricity Market. [online]. Available: https://www.nordicenergyregulators.org/about-nordreg/an-overview-of-the-nordic-electricity-market/
[36] Solar PV module prices, Our World in Data. [Online]. Available: https://ourworldindata.org/grapher/solar-pv-prices.
[37] Ryan H Wiser et al., Forecasting Wind Energy Costs and Cost Drivers: The Views of the World's Leading Experts, Berkelly Lab. [Online]. Available: https://emp.lbl.gov/publications/forecasting-wind-energy-costs-and.
[38] Ryan Wiser et al., Reducing Wind Energy Costs through Increased Turbine Size: Is the Sky the Limit?, Berkelly Lab. [Online]. Available: https://eta-publications.lbl.gov/sites/default/files/scaling_turbines.pdf.
[39] Decentralised solutions, Vattenfall. [Online]. Available: https://group.vattenfall.com/what-we-do/roadmap-to-fossil-freedom/decentralised-solutions/energy-storage.
[40] Annual change in renewable energy generation, Our World in Data. [Online]. Available: https://ourworldindata.org/grapher/annual-change-renewables?tab=chart.
[41] V. Ajjarapu and B. Lee, "Bibliography on voltage stability," in IEEE Transactions on Power Systems, vol. 13, no. 1, pp. 115-125, Feb. 1998, doi: 10.1109/59.651622.
[42] Taylor CW, "Power System Voltage Stability", McGraw-Hill, New Yord-1994.
[43] Sweden to reach its 2030 renewable energy target this year, World Economic Forum. [Online]. Available: https://www.weforum.org/agenda/2018/07/sweden-to-reach-its-2030-renewable-energy-target-this-year/.
[44] Sweden's Future Electrical Grid – a project report, 2017. [Online]. Available: https://www.iva.se/en/published/swedens-future-electrical-grid–a-project-report.
[45] Wooyoung Choi et al. Reviews on Grid-Connected Inverter, Utility-Scaled Battery Energy Storage System, and Vehicle-to-Grid Application – Challenges and Opportunities, 2017.
[46] Matthew T. Lawder et al. Battery Energy Storage System (BESS) and Battery Management System (BMS) for Grid-Scale Applications. [Online]. Available: https://ieeexplore.ieee.org/stamp/stamp.jsp?tp=&arnumber=6811152
[47] https://en.wikipedia.org/wiki/Lithium-ion_battery#Positive_electrode

[48] https://www.energy.gov/eere/articles/how-does-lithium-ion-battery-work

[49] https://hal-cea.archives-ouvertes.fr/cea-01791260/document

[50] https://www.intechopen.com/chapters/55442

[51] Alejandro Clemente and Ramon Costa-Castelló. Redox Flow Batteries: A Literature Review Oriented to Automatic Control.

[52] https://spectrum.ieee.org/its-big-and-longlived-and-it-wont-catch-fire-the-vanadium-redoxflow-battery

[53] How to use Life Cycle Costing. Available from: https://www.patriotsoftware.com/blog/accounting/life-cycle-costing-process/

[54] Beatrice Marchi et. al,. Life cycle cost analysis for BESS optimal sizing.

[55] Svenska Kraftnät, [Online]. Available: https://www.svk.se/en/national-grid/map-of-the-national-grid/

[56] Anton Thorslund, Swedish Transmission Grid Model Based on Open Sources. [Online]. Available: https://publications.lib.chalmers.se/records/fulltext/253005/253005.pdf

[57] Sharon Müller, Development of Nordic 32 system model and performance analysis based on real operation statistics. [Online]. Available: http://www.diva-portal.org/smash/get/diva2:1395253/FULLTEXT01.pdf

[58] T. Van Cutsem et al., "Test Systems for Voltage Stability Studies," in IEEE Transactions on Power Systems, vol. 35, no. 5, pp. 4078-4087, Sept. 2020, doi: 10.1109/TPWRS.2020.2976834.

[59] Program Application Guide Volume 2, PSS®E 35.0.0, September 2019.

[60] Abram Perdana, "Wind Turbine Models for Power System Stability Studies," 2006, [Online]. Available: https://core.ac.uk/download/pdf/70566696.pdf

[61] Goncalo Miguel Gloria et. al., Battery Energy Storage System in a 100% renewable network. Case study of Brava Island.

[62] Choi, Woo Yeong & Kook, Kyung & Yu, Ga. (2019). Control Strategy of BESS for Providing Both Virtual Inertia and Primary Frequency Response in the Korean Power System. Energies. 12. 4060. 10.3390/en12214060.

[63] Ming-Shun Lu, Combining the wind power generation system with energy sto rage equipments. [Online]. Available:https://rc.library.uta.edu/uta-ir/bitstream/handle/10106/1894/Lu_uta_2502M_10010.pdf?sequence=1&isAllowed=y

[64] Sunniva Bjelland, Impact of Location of Frequency Reserves. [Online]. Available: https://ntnuopen.ntnu.no/ntnu-xmlui/bitstream/handle/11250/2616425/no.ntnu:inspera:1903160.pdf?sequence=1

[65] Application Program Interface (API) PSS®E 34.3.1, October 2017

[66] Johan Lindahl and Jeffrey Berard, National Survey Report of PV Power Applications in Sweden (2019), International Energy Agency (IEA). [online]. Available: https://iea-pvps.org/wp-content/uploads/2020/08/National-Survey-Report-of-PV-Power-Applications-in-Sweden-2019.pdf

[67] The statistics and forecast, SWEA, Swedish Wind Energy Association - Svensk Vindenergi (2020-05-04). [online]. Available: https://svenskvindenergi.org/wp-content/uploads/2020/05/Statistics-and-forecast-Svensk-Vindenergi-2020-05-04-1.pdf

[68] Staffan Jacobsson et al. , Towards a strategy for offshore wind power in Sweden . [online]. Available: https://publications.lib.chalmers.se/records/fulltext/206226/local_206226.pdf
[69] Mirza Hamidovic & Mohammad Fateh Khoudeir. Load Model Identification and Parameter Estimation. Available from: https://odr.chalmers.se/bitstream/20.500.12380/300596/1/Master_Thesis_Main_ReportHamidovic_Khoudeir.pdf
[70] Photovoltaic Electricity Potential. [online]. Available: https://solargis.com/maps-and-gis-data/download/sweden
[71] Capacity adequacy in the Nordic electricity market, THEMA Consulting Group [Online]. Available: http://dx.doi.org/10.6027/TN2015-560.
[72] ESett. Nordic Imbalance Settlement Handbook Instructions and Rules for Market Participants 21 th of March 2016. (April), 2016.
[73] Daniel Hsing Po Kang et al., Potential Environmental and Human Health Impacts of Rechargeable Lithium Batteries in Electronic Waste, Environmental Science & Technology 2013 47 (10), 5495-5503 DOI: 10.1021/es400614y.
[74] FINGRID open source platform. Available from: https://data.fingrid.fi/open-data-forms/search/en/
[75] Richard Baxter, Mustang Prairie Energy, December 2020. Technology Cost and Performance Assessment.
[76] How often is the frequency within the activation area of FCR?, Svenska Kraftnät. Available from: https://www.svk.se/en/stakeholder-portal/Electricity-market/information-about-ancillary-services/questions-on-ancillary-services/fcr/how-often-is-the-frequency-within-the-activation-area-of-fcr/
[77] 'Balancing markets-business opportunity for datacenters', Svenska Kraftnät, [Online]. Available: shorturl.at/dJP47.
[78] Jacob Dalton, Optimal Day-Ahead Scheduling & Bidding Strategy of Risk-Averse Electric Vehicle Aggregator, [Online]. Available: https://www.diva-portal.org/smash/get/diva2:1249791/FULLTEXT01.pdf.
[79] Florian Hacker et al., Environmental impacts and impact on the electricity market of a large scale introduction of electric cars in Europe - Critical Review of Literature ETC/ACC TEchnical Paper 2009/4.
[80] Trade and Pricing. [Online]. Available: https://www.svk.se/siteassets/4.aktorsportalen/systemdrift-o-elmarknad/information-om-stodtjanster/trade-and-pricing.pdf
[81] Model Library PSS®E 35.0.0, September 2019.

A

Appendix

Type-4 Wind Turbine model dynamic data:

201 'WT4G1' 1 0.2E-01 0.2E-01 0.4 0.9 1.11 1.2 2.0 2.0 0.2E-01 /
201 'WT4E1' 1 0 0 1 0 0.15 18.0 5.0 0.5E-01 0.1 0.0 0.8E-01 0.47 -0.47 1.1 0.0 0.5 -0.5 0.5E-01 0.1 0.9 1.1 120.0 0.5E-01 0.5E-01 1.7 1.11 1.11 /

Type-4 Solar PV dynamic model data:

101 'USRMDL' 1 'PVGU1' 101 1 0 9 3 3 0.2E-01 0.2E-01 0.4 0.9 1.11 1.2 2.0 2.0 0.2E-01 /
101 'USRMDL' 1 'PVEU1' 102 0 4 24 10 4 0 0 1 1 0.15 18.0 5.0 0.5E-01 0.10 0.0 0.8E-01 0.47 -0.47 1.10 0.0 0.50 -0.50 0.5E-01 0.10 0.90 1.10 120 0.5E-01 0.5E-01 1.70 1.1100 1.1100 1000.0 /
101 'USRMDL' 1 'PANELU1' 103 0 0 5 0 1 0.16 0.38 0.59 0.85 1000 /
101 'USRMDL' 1 'IRRADU1' 104 0 1 20 0 1 0 0.0 1000 10 1000 15 1000 20 1000 25 1000 30 1000 35 1000 40 1000 45 1000 50 1000 /

CBEST model dynamic data:

301 'CBEST' 1 1.0 1.1 0.9 1.0 0.0 0.5 0.5 0.5 0.5 +9999 -9999 0.05/

DEPARTMENT OF SOME SUBJECT OR TECHNOLOGY
CHALMERS UNIVERSITY OF TECHNOLOGY
Gothenburg, Sweden
www.chalmers.se

CHALMERS
UNIVERSITY OF TECHNOLOGY